

THE DISCOVERY OF QUASISOFT AND SUPERSOFT SOURCES IN EXTERNAL GALAXIES

R. DI STEFANO^{1,2}, A. K. H. KONG¹¹ Harvard-Smithsonian Center for Astrophysics, 60 Garden Street, Cambridge, MA 02138² Department of Physics and Astronomy, Tufts University, Medford, MA 02155*Draft version September 15, 2018*

ABSTRACT

We apply a uniform procedure to select very soft sources from point sources observed by *Chandra* in 4 galaxies. This sample includes one elliptical galaxy (NGC 4967), 2 face-on spirals (M101 and M83), and an interacting galaxy (M51). We report on some intriguing results, including the following.

(1) We have found very soft X-ray sources (VSSs) in every galaxy. Some of these fit the criteria for canonical supersoft sources (SSSs), while others are somewhat harder. These latter have characteristic values of $kT \lesssim 300$ eV; we refer to them as quasisoft sources (QSSs). We found a combined total of 149 VSSs in the 4 galaxies we considered; 77 were SSSs and 72 were QSSs.

(2) The data are consistent with the existence of a large VSS population, most of whose members we cannot observe due to the effects of distance and obscuration. The total VSS population of sources with $L > 10^{37}$ erg s⁻¹ in each galaxy could be on the order of 1000.

(3) Whereas in M31 only $\sim 10\%$ of all X-ray sources detected by *Chandra* are VSSs, more than 35% of all detectable X-ray sources in the face-on galaxy M101 fit the phenomenological definition of VSSs. This difference may be due to differences in N_H between typical lines of sight to sources in each galaxy.

(4) SSSs can be super-Eddington for Chandrasekhar mass objects.

(5) We find evidence for SSSs and QSSs with luminosities 10^{36} erg s⁻¹ $< L < 10^{37}$ erg s⁻¹. These sources have luminosities lower than those of the ~ 30 soft sources used to establish the class of SSSs.

(6) In the spiral galaxies M101, M83 and M51, a large fraction of the SSSs and QSSs appear to be associated with the spiral arms. This may indicate that some SSSs are young systems, possibly younger than 10^8 years.

(7) In addition to finding hot white dwarfs and soft X-ray binaries, our method should also be efficient at selecting supernova remnants (SNRs). A small fraction of the VSSs in the spiral arms of M101 appear to be associated with SNRs.

Subject headings: black hole physics — galaxies: individual (M101, M83, M51, NGC 4697) — supernova remnants — white dwarfs — X-rays: binaries — X-rays: galaxies

1. INTRODUCTION

Chandra and *XMM* observations make it possible to systematically discover and study very soft X-ray sources (VSSs) in external galaxies. Until now, the canonical examples of VSSs were luminous supersoft X-ray sources (SSS). The SSSs that established the class lie in the Magellanic Clouds and in the Milky Way; they have kT in the range of tens of eV and luminosities between roughly 10^{37} erg s⁻¹ and a few times 10^{38} erg s⁻¹. *Chandra* and *XMM* surveys in other galaxies are important, since gas obscures more than 99% of the Milky Way's SSSs, so that direct studies of the size and characteristics of galactic populations of SSSs can be carried out only in other galaxies.

This paper is the third in a series on the selection of VSSs in external galaxies. In paper 1 (Di Stefano & Kong 2003a), we presented a set of strict hardness ratio conditions (the “HR conditions) to select only the softest sources. Sources selected by the HR conditions are likely to have spectra very similar to those of the SSSs observed in the Galaxy and Magellanic Clouds. Also in paper 1 we tested the HR conditions by applying them to *Chandra* data from 4 galaxies. In paper 2 (Di Stefano & Kong 2003b), we presented an algorithm that starts with the HR conditions, but which then proceeds to progressively relax them. Each set of relaxed conditions chooses sources that deviate from the expected broadband spectra of SSSs in some way. For example, the 3σ conditions select sources that may be as soft as SSS-HRs, but which provide too few photons to satisfy the stronger HR conditions. Any source satisfying

either the HR or 3σ conditions is called a classical supersoft source, or simply an SSS (SSS-HR or SSS- 3σ). In addition, there is a set of 7 conditions which can select either highly absorbed SSSs, or sources that are genuinely harder than the SSSs studied in the Galaxy and Magellanic Clouds. We refer to any source which satisfies one of these weaker conditions as a quasisoft source (QSS). For example, the “NOH” conditions can select quasisoft sources (QSS-NOH) located behind large gas columns. Other conditions (e.g., the “ σ ” conditions) select sources (QSS- σ) which may have a dominant component as soft as SSSs, but which also include a small hard component. All sources selected by the algorithm, whether they are supersoft or quasisoft, are referred to as very soft sources (VSSs).

In this paper, we apply the full algorithm to data from the same 4 galaxies considered in paper 1: M101, M83, M51, and NGC 4472. Because the HR conditions have already been applied, we could have left SSS-HR sources out of this analysis. We decided however, to include them, because it is useful to explicitly compare their properties with those of the other soft sources identified by higher steps in the algorithm.

2. DATA ANALYSIS

For M101 and M51, we generated our own source lists with the CIAO tool WAVDETECT. For M83 we used a source list provided Soria & Wu (2003), and for NGC 4697 we used the source list of Sarazin et al. (2001). For M101 and M51, we set the input parameters for WAVDETECT to cover the en-

ergy range 0.1–7 keV. For galaxies in which the lower energy limit used by WAVDETECT was greater than 0.1 keV, we carried out a visual inspection to search for any sources with reliable detections but with few photons detected above 0.3 keV. Source counts in each energy band were determined via aperture photometry. The radius of the aperture was varied with off-axis angle in order to match the 90% encircled energy function. Background was chosen from an annulus region centered on each source. We note that, while the calibration at the lowest energies ($kT < 0.3$ keV) will need to be refined for spectral fits, source detection algorithms should include photons with energies as low as 0.1 keV if all SSSs and QSSs are to be detected. In 3 of the galaxies, photons with energies between 0.1 keV and 0.3 keV have helped to detect a small number of SSSs and QSSs. Because visual inspection of each source must be carried out anyway, any spurious sources detected because of background effects at low energy can be easily eliminated.

In addition to estimates of the number of background objects based on the *Chandra* Deep Field data (see the references in each of the galaxies below), we also used the ChaMP (*Chandra* Multiwavelength Project¹) archives (P. Green, private communication) to estimate the contamination from soft X-ray sources in the foreground (X-ray active stars) and background (e.g., soft AGN). In 5 ACIS-S observations with durations of ~ 10 –20 ks, only 3 sources were found to be QSSs; no SSSs were identified. We therefore believe that the background contribution of soft sources is small compared with the large population of SSSs in our sample galaxies.

2.1. The Sources

2.1.1. M101

M101 (= NGC5457) is a face-on nearby (5.4–6.7 Mpc) spiral and was observed by *Chandra* ACIS-S for about 100ks on 2000 March 26–27. Detailed results of the observations have been reported by Pence et al. (2001). We generated our own source list here with CIAO task WAVDETECT instead of CELLDTECT used by Pence et al. (2001). We also used different energy bands covering 0.1–7 keV, instead of 0.125–8 keV in Pence et al. (2001). Pence et al. (2001) estimated that 27 sources are possible background AGN. While the source lists agree with each other generally, we found 8 additional sources (118 in total) in the S3 chip. The list of SSSs and QSSs is shown in Table 2. We found a total of 53 VSSs; 32 were SSSs and 21 were QSSs.

2.1.2. M83

M83 (= NGC5236) is a barred spiral galaxy with low inclination angle ($i = 24^\circ$); it has a starburst nucleus and the estimated distance ranges from 3.7 Mpc to 8.9 Mpc. A *Chandra* ACIS-S observation was taken on 2000 April 29 for about 50ks. The X-ray point source properties and the nuclear region were discussed by Soria and Wu (2002, 2003). One hundred and twenty seven point sources were found in the S3 chip (0.3–8 keV) and approximately 10 sources are likely to be background AGN. We used this source list for our analysis. In addition, visual inspection from a 0.1–1 keV image discovered 1 new SSS. Table 3

lists M83's SSSs and QSSs. We found a total of 54 VSSs; 28 were SSSs and 26 were QSSs.

2.1.3. M51

M51 (= NGC5194) is a nearby (7.7–8.4 Mpc) interacting spiral galaxy with moderate inclination ($i = 46^\circ$). A *Chandra* ACIS-S observation was performed on 2000 June 20 for about 15ks. A detailed analysis of the data is given by Terashima & Wilson (2003). We generated our own source list with the CIAO task WAVDETECT. A total of 72 sources (in 0.3–7 keV) were found in the S3 chip. About 10 of the sources are expected to be background objects. All SSSs and QSSs are listed in Table 4. We found a total of 23 VSSs; 13 were SSSs and 10 were QSSs.

2.1.4. NGC4697

NGC4697 is an elliptical galaxy at a distance of 11.7–23.3 Mpc. It was observed by *Chandra* ACIS-S on 2000 January 15–16 for about 40ks. Ninety point sources were detected in the S3 chip (0.3–10 keV; Sarazin, Irwin, & Bregman 2001); about 10–15 background objects are expected in the observation. The complete source list and results from this observation can be found in Sarazin et al. (2001). We also inspected an image from 0.1–1 keV and found 1 new uncatalogued SSS. Table 5 lists the SSSs and QSSs found with our selection procedure. We found a total of 19 VSSs; 4 were SSSs and 15 were QSSs.

2.2. Spectra of Very Soft Sources

2.2.1. The Spectra

Individual Sources: To determine whether our algorithm selects sources that are genuinely soft, we have extracted the energy spectra of all very soft sources that provided more than ~ 200 counts. Background counts were extracted in annulus regions centered on each source. There are 10 such sources. We have also considered the spectra of sources with more than 100 counts, although the uncertainties in spectral parameters are large. A representative spectrum of a QSS- σ source is shown in Figure 1. The spectral fits are listed in Table 6.

Composite Spectra: Because many VSSs are faint, fits of individual spectra are not possible. If, therefore, we found a number of sources that (1) had been identified by the same criteria, and which (2) displayed similar broadband spectra and (3) provided a total of approximately 100 counts, we extracted the composite energy spectra (see e.g., Figure 1).

Because the response matrices vary across the detector, a weighted RMF and ARF was generated following the thread recommended by the *Chandra* X-ray Center². Results are presented together with the individual spectra in Table 6.

The analysis of *Chandra* spectra of VSSs is fraught with uncertainties because the low-energy ($kT < 0.5$ keV) calibration of ACIS-S is not yet well understood³. It is therefore important to keep in mind that the spectral fits of SSSs, especially those that peak at energies near or below 0.5 keV are not on the same footing as the spectral fits of higher-energy sources, and may need to be reanalyzed once the low-energy calibration has been better studied.

¹ <http://hea-www.harvard.edu/CHAMP>

² http://asc.harvard.edu/ciao/threads/wresp_multiple_sources

³ We have, e.g., data on all of the nearby SSSs, and find anomalous behavior at low energies that appears to be related to the difficulties encountered so far with the low-energy calibration. Some of these anomalies would be less obvious in the distant sources we discuss here, because the total number of counts is generally relatively small; calibration uncertainties may nevertheless affect the derived values of spectral parameters.

We also note that the quantum efficiency degradation of ACIS at low energies is important for SSSs and QSSs. The degradation has been shown to be a function of time and is most severe at low energies⁴. For a source with blackbody temperature of 100 eV and $N_H = 10^{20} \text{ cm}^{-2}$, the ACIS-S counts below 2 keV had dropped by about 30% one year after the launch and by almost 50% after two years (P. Plucinsky, private communication). Fortunately this problem has been well studied and it is possible to take the effect into account. We therefore applied corrections using the ACISABS absorption model in XSPEC⁵. This model allows us to correct the response by inputting the number of days between *Chandra*'s launch and the observation. We find that, for very soft sources, the degradation mainly affects the best fit value of N_H ; the uncorrected model tends to over-estimate the value (see also Kong et al. 2002).

For each spectral fit, we selected photons within a circular region centered on the source. Only 0.3–7 keV data were used. We first fit the spectra with simple one-component models including absorbed power-law, blackbody and Raymond-Smith (RS) models. In all but three cases, an absorbed blackbody model can provide a good fit. For the three exceptional spectra, we added an additional power-law component or fit with a RS model in order to derive an acceptable result.

Table 6 shows that, as expected, sources satisfying the HR conditions are generally the softest. While the other sources tend to be harder, all but 1 satisfy the conditions used to define VSSs (Di Stefano & Kong 2003a); M51-10 appears to be marginally harder. We note one unusual feature. This is that, in each galaxy, typical values of N_H associated with the fits of QSSs are significantly higher than the minimum value of N_H along the direction to the galaxy. If, however, internal absorption is not a significant factor for most SSSs and QSSs, the distribution of N_H should mirror the spatial distribution of SSSs along the line of sight within the galaxy. That is, since SSSs and QSSs are generally expected to be evenly distributed along the line of sight, values of N_H should range from approximately N_H^G , the Galactic value along that line of sight to a high of $\sim N_H^G + (z \cdot 3.08 \times 10^{18}) / \cos\theta$, where z is the scale height of the galaxy (in pc) and θ is the angle between the normal to the galactic plane and the line of sight. (We have assumed that, within the galaxy, there is on average one hydrogen atom per cubic cm.) For the galaxies we have studied, this generally means that N_H should range from a few times 10^{20} cm^{-2} to a few times 10^{21} cm^{-2} . Because absorption interferes with very soft source detection, we expect a bias toward values of N_H on the lower end of this range. Yet, the values of N_H associated with the QSS fits summarized in Table 6 tend toward the high end. This could imply that internal absorption is generally high in QSSs. We note however that it is also possible that there is a systematic bias in the fits, perhaps due to an overestimate of the efficiency with which ACIS is detecting soft X-ray photons. (See also §5.3.2.) Improvements in the low-energy calibration are required to resolve this issue.

2.2.2. Special Cases

M101-102 is an ultraluminous SSS ($L_X \sim 4 \times 10^{39} \text{ erg s}^{-1}$). No one-component model provides an acceptable fit. We therefore fit the spectrum with an absorbed blackbody plus RS model. We found that the 91 eV blackbody component contribute 85% of the X-ray emission in 0.3–7 keV. This source

⁴ see http://asc.harvard.edu/cal/Links/Acis/acis/Cal_prods/qeDeg/

⁵ <http://www.astro.psu.edu/users/chartas/xcontdir/xcont.html>

has recently been studied by Mukai et al. (2002), Di Stefano & Kong (2003a) and Kong & Di Stefano (2004).

In 2 other cases, blackbody models did not provide acceptable fits. M101-53, a QSS, found by applying the “ σ ” condition, can be fit by a RS model with $kT_{RS} = 0.64 \text{ keV}$. A composite of QSS-SNOH sources in M101 requires a two-component model (RS plus power-law). The RS temperature is 0.25 keV and the photon index of power-law is 2.4; the thermal component contributes about 22% of X-ray emission. We suspect that M101-53 and one or more of the SNOH sources comprising the composite may be supernova remnants.

Four QSS candidates in M83 (M83-116, M83-117, M83-119 and M83-120) are near the nucleus where the diffuse emission contaminates the source spectra. Moreover, M83-116, M83-117 and M83-119 are near ($\sim 1''$) to each other while M83-120 has a nearby bright X-ray source. These circumstances make the spectral analyses difficult, and we therefore took special steps to fit the spectra of these sources. In each case, in addition to the source spectrum, we also extracted a spectrum from a source-free region in an adjacent area with diffuse emission. We used this latter as background. After background (diffuse emission) subtraction, we fit the spectra with single-component models and the results are listed in Table 6. Blackbody models with temperatures of $\sim 140 \text{ eV}$ gave acceptable fits to M83-116 and M83-119. For M83-117 and M83-120, the background appeared to be over-subtracted and no single- or two-component model provided a good fit. We therefore considered the source spectrum without background subtraction and fit a two-component model (MEKAL + blackbody). The MEKAL component represents the contribution of the diffuse emission (see Soria & Wu 2002) while the blackbody component corresponds to the spectrum of the point source. Table 6 lists the best-fit results. The MEKAL plasma temperature is roughly consistent with the value for the diffuse emission found previously (Soria & Wu 2002) while the blackbody temperature is about 60 eV. The flux contribution of the blackbody component is 82% and 43% for M83-117 and M83-120, respectively.

2.2.3. Tests of the Selection Algorithm

SSSs: The spectral fits allow us to determine what sorts of sources are selected by our algorithm. As expected, the HR conditions are the most stringent. When applied to M101, M83, M51, and NGC 4697, they identified sources that have $kT \lesssim 100 \text{ eV}$. Even for the ultraluminous source in M101 (M101-102), which required a two-component fit, fewer than 2% of the energy was emitted in the form of photons with energies above 1.5 keV. In addition, the values of N_H among the HR-identified sources are distributed more-or-less uniformly between a few $\times 10^{20} \text{ cm}^{-2}$ and a few $\times 10^{21} \text{ cm}^{-2}$, roughly consistent with the expected distribution of obscuring gas. Thus, the HR conditions seem to identify sources with the spectral characteristics expected of classical SSSs.

The SSS category encompasses both SSS-HRs and SSS- 3σ s. The SSS- 3σ category should consist of very soft sources with count rates too low to allow the straight HR conditions to be satisfied. In the 4 galaxies, no SSS- 3σ provided enough enough photons to allow a spectral fit. To carry out a fit we therefore considered a composite of 7 SSS- 3σ sources. Although this composite spectrum appears to be significantly harder than the

SSS-HRs, both the formal and systematic uncertainties (the latter largely associated with creating the composite spectrum) are large. We therefore note that our results on SSSs are dominated by the bright SSS-HRs in our sample.

QSS: We were able to derive fits for 10 QSSs and 3 QSS-composites identified by using other conditions. As is to be expected, the photon statistics were generally not quite as good for sources identified via the other conditions, and the uncertainties in the spectral parameters are greater.⁶ The fits of two of these spectra (M101-53, and the SNOH composite in M101) seem compatible with what we might expect for SNRs. For the other spectra, the best-fit temperatures are generally higher than for sources in the HR category. Nevertheless, with just one exception, $kT < 175$ eV.

Comparison: The QSS spectra are generally harder and the values of N_H appear to be systematically higher. In fact 7 of the fits yield values of N_H larger than the largest value derived for HR-identified sources. In at least 3 cases, internal absorption would have to be very significant, or the gas would have to be associated with a high-gas-density region, in order for the derived values of N_H to be physical. This could be a genuine selection effect, since some of these categories were especially designed to allow us to identify SSSs located behind large gas columns, which could be associated with the system or which could be spread out along the line of sight.

2.3. Luminosity

2.3.1. Luminosities

When spectral fits are possible for only a small fraction of sources in an external galaxy, the luminosity function is usually computed by assuming that a single factor can convert the count rate of each source into an estimated source luminosity. The uncertainties can be estimated by using a set of spectral models (perhaps drawn from those that fit the high count-rate sources) to compute independent conversion factors, and using them to derive a range of physically plausible LFs. For VSSs, however, the conversion from count rate to luminosity depends critically on both the source temperature and the value of N_H . To gain insight into the distribution of luminosities we can therefore rely only on the sources for which we have spectral fits. In table 6 we list the computed luminosities for each source and composite for which we derived spectral fits. For each source we list both a low value of the luminosity (assuming that the galaxy's distance from us is the minimum listed in Table 1) and a high value (assuming that the galaxy's distance from us is the maximum listed in Table 1). We have used these values to compute 1 LF for the associated VSSs using the lower distance estimate. For those sources that are composites, we have assumed that the spectra of the sources contributing to the composite are similar. We have therefore assigned to each source a fraction of the total luminosity that is equal to the fraction of the total counts contributed by that source. In total, 40 sources contribute to our LF: 14 single sources and 26 sources whose luminosities were determined by studying the spectrum of a composite to which they contributed. The results are shown in Figure 2.

While the function shown in Figure 2 displays some interesting-looking features, it is not possible to compare it directly to the LFs of galactic populations of harder sources. Per-

haps the largest uncertainty is that we do not know how well our assumed distribution of luminosities for sources comprising composites reflects reality. In addition, for some of the composites, the temperatures and luminosities are not very well constrained. Finally, we do not know how well this distribution reflects the characteristics of the dimmer sources in our sample. Nevertheless there are a few noteworthy features. Among the sources in this sample, about 18% have $L < 10^{37}$ ergs s⁻¹ and 27% of the sources have $L > 10^{38}$ ergs s⁻¹.

Referring to Table 6, we find that the low-luminosity sources ($L < 10^{37}$ ergs s⁻¹) tend to have high temperatures, between 80 and 170 eV. The high temperature of the low-luminosity sources is a selection effect—we simply would not have detected these sources had their temperatures been well under 100 eV. It is, however, interesting that there are low-luminosity sources with such high temperatures. One of the predictions of nuclear-burning WD models is that the luminosities and temperatures are larger for WDs of higher mass. Low-L/high-T sources do not seem to fit this pattern. Given the uncertainties in the spectral parameters, and the assumptions made about the composite spectra, it may be too early to conclude that the apparent low-L/high-T sources are not nuclear-burning white dwarfs (NB-WDs). But the data do suggest that these systems may be described by a different physical model.

2.3.2. Count Rates

Figure 3 shows, for each galaxy, the distribution of count rates for VSSs (red) and for all other sources (black). There are no obvious breaks in the distributions as we approach lower count rates. This indicates that, if we had longer and/or more sensitive observations, we would detect both VSSs and other sources that are even dimmer than the sources discovered so far.

In general, there are fewer VSSs than non-VSSs in each galaxy. This is especially true for NGC 4697 and M51. There is nevertheless some preliminary evidence that count-rate distribution for VSSs in each galaxy is more sparsely populated at high-count-rates. This makes the few high-count-rates SSSs particularly interesting.

2.3.3. Ultraluminous SSSs

One of the VSSs is clearly an ultraluminous X-ray source (ULX). With a luminosity that appears to be larger than 4×10^{39} ergs s⁻¹, M101-102 (a HR source) is clearly super-Eddington for a neutron star. It cannot be explained by a NBWD model. Three of the sources in NGC 4697 are also particularly luminous. The 3 sources comprising the HR composite in NGC 4697 are roughly equally bright. The luminosities of the individual sources would therefore be $\sim 10^{38}$ ergs s⁻¹ if the distance to NGC 4697 is 11.7 Mpc, but they could be as high as $\sim 4 \times 10^{38}$ ergs s⁻¹ if the distance to NGC 4697 is 23.3 Mpc. If the true luminosities are sub-Eddington for a $1.4M_\odot$ object, then these systems could include NBWDs that are both hot and bright because they are approaching the Chandrasekhar limit. Since super-Eddington luminosities can occur during short-lived states (e.g., in Nova LMC 1990#1; see Vanlandingham et al. 1999), it will be important to study the time variability properties of such luminous soft sources.

⁶ There were a relatively large number of photons associated with each of the sources near the center of M83, but the effects of the diffuse emission introduce additional uncertainties.

2.4. Location

Identifying very soft sources in external galaxies allows us to determine their locations relative to galaxy populations of young and old stars and also relative to the nucleus, spiral arms, and other galactic structures. This information can in turn, provide valuable clues to the natures of the sources.

2.4.1. Near the Galaxy Centers

It is impossible to detect the soft X-radiation from any SSSs/QSSs that may be near the center of the Milky Way. Furthermore, because the nature(s) of the sources are not well understood, there were no predictions about whether we should find SSSs/QSSs near galaxy centers. In M51, we excluded the inner $15''$ because of possible contamination from the central AGN. In each of the other 3 galaxies, we would have discovered any SSSs located near the center. Only M83 has SSSs/QSSs within 100 pc of the galaxy center. The 3 sources identified by the σ conditions, M83-116, M83-117, and M83-120 are within $45''$ of the nucleus. Because of possible contamination from the diffuse emission, it will require further study to determine if these are genuine point sources.

All of the galaxies in our sample have VSSs within 1 kpc of the center. The significance of the value of 1 kpc is that this is the distance a source moving at an average speed of 200 km s^{-1} could travel in 5 million years. If a very soft source is the stripped core of a tidally disrupted giant, then its maximum lifetime as a soft source should be approximately $10^3 - 10^6$ years (Di Stefano et al. 2001).

M101: There are 2 SSSs and 2 QSSs within 1 kpc; 2 of these were selected by the HR conditions, 1 by HR1, and one by $3\sigma_1$. There are 5 additional X-ray sources within 1 kpc.

M83: There are 9 SSSs and QSSs within 1 kpc; 1 HR, 1 3σ source, 4 σ sources, and, 3 HR₁. That same region contains a total of 24 X-ray sources. We note however, that the *only* sources within 100 pc of the center are very soft sources, suggesting that it is important to verify or falsify the point-like nature of these diffuse-emission-contaminated sources.

M51: There is just one (QSS- $3\sigma_1$) source within 1 kpc of the center of M51, while there is a total of 3 X-ray sources in this region.

NGC 4697: 1 SSS and 4 QSSs (1 HR, 3 SNOH, and 1 HR₁) are located within 1 kpc of the galaxy center. Only 14% of all of NGC 4697's X-ray sources are located within 1 kpc of the center.

These results are summarized in Table 7, where we also compute a central concentration factor for both very soft sources and all X-ray sources. Let $f_{\text{SSS+QSS}}(\text{fall})$ represent the fraction of very soft sources (all X-ray sources) found within 1 kpc of the galaxy's center. In addition, let f_{area} be the fraction of the galaxy's total surface area comprised by a 1 kpc disk. The concentration factor for SSSs, $\mathcal{F}_{\text{SSS+QSS}}$, is computed as follows.

$$\mathcal{F}_{\text{SSS+QSS}} = \frac{f_{\text{SSS+QSS}}}{f_{\text{area}}} \quad (1)$$

Table 7 demonstrates that X-ray sources are centrally concentrated in all 4 galaxies. It also demonstrates significant differences among the galaxies, with relatively mild central concentration ($\mathcal{F}_{\text{SSS+QSS}} = 15$) in M101, moderate concentration ($\mathcal{F}_{\text{SSS+QSS}} = 50$) in M83 and M51, and heavy concentration concentration ($\mathcal{F}_{\text{SSS+QSS}} = 360$) in NGC 4697. Only in NGC 4697 are the SSSs significantly more centrally concentrated than other X-ray sources. These results suggest that a

more complete study is warranted. More galaxies need to be included and the fall off of optical light versus X-ray source density should be studied. Since the central regions are dense in sources of optical light, comparing the X-ray source distribution to that of optical light could provide insight into the mechanisms by which the X-ray sources are produced.

2.4.2. In the Spiral Arms

Superposing the positions of the SSSs and QSSs on optical images of each of the 3 spiral galaxies produces an impression that a large fraction of the SSSs and QSSs are in the spiral arms. (See Figure 4 for all of the sources and Figure 5 for those sources with spectral fits.) In most cases, populations found in the spiral arms are young populations, with ages on the order of 10^8 years. If, therefore, SSSs are primarily associated with WDs orbiting low-mass ($< 2.5 M_{\odot}$) companions, we would not expect them to be a spiral arm population, but to be spread across the face of the galaxies in a manner that resembles the distributions of planetary nebulae (PNe) or recent novae. (Indeed, we expect some SSSs to be central stars of PNe or to be recent novae.)

Old populations or intermediate age populations (with current ages greater than a few times 10^8 years), should not be primarily associated with spiral arms. Certainly we expect some of the systems we have observed as SSSs to be old. Novae, for example, should be scattered throughout the body of each galaxy. In addition, because the donors in symbiotics are giants with masses typically below $2 M_{\odot}$ (Kenyon 1986), they should also be older than $\sim 10^9$ years. 4 of 9 Galactic SSSs with optical IDs are either novae or symbiotics, as is 1 of 3 SMC SSSs with optical IDs, and 1 of 7 LMC SSSs with optical IDs. One SSS and 1 QSS in M31 are tentatively identified with symbiotics (Di Stefano et al. 2003), as is 1 nova (Nedialkov et al. 2002); these constitute the only optical IDs of SSSs in M31. Of the remaining 13 SSSs with optical IDs in the Magellanic Clouds and Galaxy, 9 are candidates for the close-binary super-soft source (CBSS) model. The donors in CBSSs are thought to main sequence or slightly evolved stars with M below approximately $2.5 M_{\odot}$. Whether the donor is slightly evolved or on the main sequence, the ages of the systems at the time mass transfer begins the SSS phase is typically larger than 10^8 years. Thus, although detailed population synthesis computations are needed to quantify the relationship between location, level of activity, and age, it seems clear that most WD SSSs (with the possible exceptions of very hot central stars of planetary nebulae descended from massive stars, or accretors of heavy winds from massive companions) should not be part of young populations.

More convincing than a visual impression of an association between the locations of VSSs and the spiral arms, would be a meaningful statistical correlation between the positions of the VSSs and the positions of markers of young populations, such as SNRs, OB associations, and HII regions. Work is underway to study these correlations in M101. Below we mention some specific cases in which SSSs are close to optical markers in M101. The results of a statistical analysis will be reported elsewhere.

Nine of the VSSs (7 SSSs and 2 QSSs) are within $10''$ (~ 240 pc, at the distance to M101) of supernova remnants (SNR; Matonick & Fesen 1997). While at this point we cannot make a convincing identification between the VSSs and the nearest SNR to each, it is likely that a subset of these 9 VSSs may

in fact be associated with SNRs, especially since all of the 7 SSSs are within 2'' (~ 48 pc) of an SNR. Astrometric study is underway to assess the likelihood of genuine identifications. Because all 9 sources have relatively low count rates, we do not have spectra.

In addition, 19 distinct VSSs (11 SSSs and 8 QSSs) are within 10'' of an HII region (Scowen et al. 1992), with one SSS located near 3 HII regions, and 2 VSSs (1 SSS and 1 QSS) each located near 2 distinct HII regions. We have spectra for 4 of these sources. M101-104 and M101-51, each identified through the strong HR conditions, are among the softest sources in our sample, with kT of 67 eV and 50 eV, respectively. M101-114 was identified through the MNOH condition, and is well fit by a $kT = 124$ eV model; the uncertainties in the fit yield a maximum value of kT of ~ 150 eV. We have conjectured that M101-53, identified through the σ condition, may be an SNR, since the best-fit model was an RS model with $kT_{RS} = 0.64$ keV. Furthermore, 1 QSS is within 10'' of a PN (Feldmeier et al. 1997).

If indeed we can establish a spatial correlation between VSSs and markers of young stellar populations, and if this correlation is significantly larger than the correlations between PNe (and novae) and markers of young stellar populations, then we will be forced to conclude that a substantial fraction of VSSs are members of relatively young stellar populations.

We must then consider whether the VSSs we are identifying are dominated by SNRs. It should be possible to distinguish SNRs from VSSs which are X-ray binaries by taking multiple X-ray images; SNRs, whose emission emanates from regions extending over several parsecs, should not be variable on time scales of months to a few years, while most other VSSs are highly variable over these time scales (Kong & DiStefano 2003a; Di Stefano & Kong 2003b; Di Stefano et al. 2003; Fabbiano et al. 2003). We note that some SSSs which are X-ray binaries are expected to be associated with ionization nebulae. If the nebulae are not too dim or too diffuse, VSSs of medium T (likely to be SNRs) and VSSs of lower- T (more similar to SSSs in the Milky Way and Magellanic Clouds) may be distinguished by various sets of line ratios (see, e.g., Rappaport et al. 1994, Di Stefano, Paerels & Rappaport 1995, Chiang & Rappaport 1996).

Even before such follow-up observations are conducted, we can conclude that it is unlikely that the VSS populations we have identified are dominated by SNRs. First, this would be counter to the trend discovered by Long et al. (1981) for the Magellanic Clouds. The 2 SSS binaries, CAL 83 and CAL 87 had hardness ratio [(H-S)/(H+S)], where S includes photons between 0.15 and 1.5 keV and H includes photons between 1.5 and 4.5 keV] of -0.9 and -0.7, respectively. No SNR is as soft as CAL 83 and only 4 are as soft or softer than CAL 87. X-ray luminosities are quoted for 3 of these SNRs, and they range from 2×10^{35} erg s $^{-1}$ to 4×10^{35} erg s $^{-1}$. They would not be detected in any of the galaxies we have studied. Although it may be the case that some SNRs have both spectra and luminosities more typical of SSS X-ray binaries (see, e.g., Kong et al. 2002; Kong et al. 2003; Swartz et al. 2002), the survey of the Magellanic Clouds is consistent with a general trend in which SNRs become larger, softer, and less luminous with time. The second reason we doubt that the VSS population we identify is dominated by SNRs, is that the total populations of VSSs in the Galaxy, the Magellanic Clouds, and in M31 are certainly not dominated by SNRs. In M31 (Di Stefano et al. 2003), the VSSs

identified by our criteria are highly variable on time scales of months to years, so that the X-ray emission cannot be coming from an extended region. (See the SSS catalog [Greiner 2000] for a summary of the properties of SSSs in the Galaxy and in the Magellanic Clouds.)

3. THE SIZE OF GALACTIC SSS POPULATIONS

The SSSs we have detected in each galaxy comprise a small fraction of all of the VSSs within the galaxy. We detect primarily the hottest, brightest VSSs. This effect becomes even more pronounced for distant galaxies and/or for (a) galaxies located along lines of sight with large values of N_H , (b) galaxies with large internal gas components, or (c) spiral galaxies with large inclination angles.

To estimate the size of the total population, we must determine what fraction of all the sources we can (1) detect and (2) identify as VSSs. The second requirement is more restrictive, as typically more than 14 photons are needed. Assuming that at least 14 photons are needed, we can compute, for each temperature and each value of N_H , the minimum luminosity of a detectable VSS in each galaxy. We have done these computations for each value of T and N_H used in the PIMMS simulations described in paper 2 (Di Stefano & Kong 2003b).

If we knew the true distribution of VSS properties (L and T , assuming that thermal models apply) and the spatial distribution of gas within each galaxy, we would be able to compute the true fraction of VSSs we should have detected and identified in each galaxy. We could even check whether the properties of the sources we actually do detect match those of the predictions. Unfortunately, however, we do not know enough about VSSs to make reliable first-principles calculations possible.

What we can say is that galactic VSS populations can productively be viewed as having 3 components.

3.1. The "classical" SSSs

The first component mirrors the SSSs studied by ROSAT to first establish the class. A significant fraction of these are candidates for binaries which include a NBWD. Distributions of source properties for this class were computed by Rappaport, Di Stefano & Smith (1994; RDS) and later used by Di Stefano & Rappaport (1994) to estimate the fraction of SSSs that the *ROSAT All-Sky Survey* had discovered in the Galaxy, M31, and the Magellanic Clouds. Although specifically constructed to mimic the distributions of CBSS properties, the RDS distributions seemed to fairly well represent the properties of all SSSs discovered during the early 1990s. (Note however, that the source properties were only established for about a dozen sources and that they were poorly constrained.)

We have used the same distribution to compute the fraction of all sources like those discovered in the early 1990s that we would have detected and identified in M101, M83, M51, and NGC 4697. To accomplish this we constructed a template of sources from the PIMMS simulations described in §3 of Di Stefano & Kong (2003a). Each source was characterized by a temperature (with kT ranging from 25 eV to 175 eV), and a value of N_H .

We then carried out a simulation in which we seeded each galaxy with the RDS distribution. The galaxy's distributions of N_H were modeled in a very simple way. For NGC 4697 we assumed a column of 4×10^{20} cm $^{-2}$ for each source. For M101 and M83 we assumed that an SSS has an equal probability of lying behind a column of 4×10^{20} cm $^{-2}$ or of 1.2×10^{21} cm $^{-2}$.

For M51, which has a higher inclination angle, we assumed that three values of N_H are equally likely: $4 \times 10^{20} \text{ cm}^{-2}$, $1.2 \times 10^{21} \text{ cm}^{-2}$, and $6.2 \times 10^{21} \text{ cm}^{-2}$.

For each galaxy, we considered each source in the RDS distribution. Comparing its temperature to the temperature of each source in the template (which is characterized by T and N_H), we computed the luminosity the source would need to have in order to yield 14 counts. If the actual source luminosity was this high or higher, we counted the source as detected.

The results are summarized in Figure 6 and in the paragraphs below. The top panel of Figure 6 shows one of the “parent” distributions of “classical” SSSs. The panels below show the members of that parent distribution that would be detected in M101, M83, M51, and NGC 4697, respectively. We have assumed that the distance to each galaxy is the average of the highest and lowest values given in Table 1. In all of these external galaxies, we can detect only the hottest and brightest sources in the distribution. This effect is, however, very pronounced in M51 and especially in NGC 4697, where we can detect only the high-L, high-T tip of the distribution.

M101 and M83: The fraction of sources we would detect ranged from 2% to 5%, with a median value of 3%. This implies that each “classical” SSS detected represents between 20 and 50 SSSs, with a median expectation value of ~ 33 .

M51: The fraction of sources we would detect ranged from 0.1% to 0.25%, with a median value of 0.17%. This implies that each “classical” SSS detected represents between 400 and 1000 M51 SSSs, with a median expectation value of ~ 590 .

NGC 4697: The fraction of sources we would detect ranged from 0.05% to 0.2%, with a median value of 0.09%. This implies that each “classical” SSS detected represents between 500 and 2000 NGC4697 SSSs, with a median expectation value of ~ 1100 .

For each galaxy we now have to estimate the number of classical SSSs detected. Given the limited information we have, it is not presently possible to do this in a reliable way. We could, for example attempt to estimate the number of SSSs that seem different from the “classical” profile and subtract these from the total number of VSSs in each galaxy, to arrive at an upper limit. We do not, however, have enough information about individual sources to make this assessment. On the other hand, the HR category does seem to select sources with temperatures in the appropriate range. Some of these, however, have luminosities that are too large. To make a conservative estimate, we utilize *only* sources in the HR category, using the total number, N_{HR} , of such sources to derive a conservative upper limit, and half of the total in HR to derive a lower limit. This is conservative because it excludes the majority of SSSs in each galaxy. It assumes that the sources identified outside of the HR condition are most likely to represent types of SSSs that are not common in the solar neighborhood or in the Magellanic Clouds.

We multiply the median expectation value for each galaxy by $N_{HR}/2$ and by $N_{HR} + N_{3\sigma}$ to derive a range for the number of “classical” SSSs. For M101 the range is from 330 to 660. For M83 the range is from 250 to 500. For M51 the range is from 1500 to 3000. For NGC 4697 the range is from 2200 to 4400.

There are 2 important caveats. First, for the galaxies that are farthest from us, these estimates would be overestimates, if none of the SSSs we detect actually have the classical profile but are instead more luminous and hotter. This would not imply that NGC 4697 doesn’t have a large “classical” SSS population, rather that we cannot estimate the size of that population based

on the data. The second caveat is that, for the spirals that may be closer to us, M101 and M83, the conservative estimates may be underestimates.

3.2. Nova-like variables and other high m CVs

The second class of SSSs we expect to inhabit distant galaxies are the low-L ($10^{35} - 10^{37} \text{ erg s}^{-1}$, low-T ($kT < 40 \text{ eV}$) sources that may be associated with nova-like variables or CVs with particularly high accretion rates—systems like V751 Cyg (Greiner et al. 1999; Patterson et al. 2001), and V Sge (Greiner & van Teeseling 1998). These systems would not be detected by the observations carried out so far, so the observations we have used here cannot constrain the sizes of these populations in the 4 galaxies we study. Nevertheless, some reasonable assumptions can be made. First, it is very likely that each of these galaxies houses a population of CVs. If the old stellar populations of the 4 galaxies in our study have similar characteristics to those of the Galaxy, we might expect there to be ~ 10 times as many low-L, low-T SSSs “on” at any given time, as there are SSSs with $L > 10^{37} \text{ erg s}^{-1}$.

3.3. New Classes of Very Soft Sources

It is clear that, among the VSSs we have identified in M101, M83, M51, and NGC 4697, there are sources unlike any found to date in the Galaxy, Magellanic Clouds, or in M31. At this point, it is difficult to estimate the size of these “new” populations. The QSSs comprise one new class. Many are hotter than the canonical SSSs, and may therefore be easier to detect; the catch, however, is that many are near the detection limits. There could be many more below the detection limits. Among the SSSs, we also find low-L sources, some with luminosities for their estimated temperatures so low that they may not be consistent with WD models. Most likely, the systems detected so far simply represent the most detectable members of the “new” SSS populations.

To be able to estimate the size of these new populations we need physical models for them, so that population synthesis simulations can produce distributions with which to seed galaxies. We also need further observations of these and of more nearby galaxies, to explore lower luminosities and temperatures.

4. DISCUSSION

The work described in this paper has served three purposes. First, it tests the selection algorithm presented in the companion paper. By fitting spectra to those sources providing adequate numbers of counts, we find that the criteria uniformly select soft sources. As expected from the tests conducted on simulated data (Di Stefano & Kong 2003a), those VSSs fit by blackbody spectra had $kT < 250 \text{ eV}$, while all VSSs emitted less than 10% of their flux in photons with energies greater than 1.5 keV. Second, we establish the existence of QSSs. Sources with kT on the order hundreds of eV and $L > 10^{36} \text{ erg s}^{-1}$ appear not to have been observed before. By now, observations in several nearby galaxies, including M31 (Di Stefano et al. 2003a) and M104 (Di Stefano et al. 2003b) verify the result. Finally, investigations have also yielded interesting information about extragalactic SSSs, providing some first steps toward answering the 7 questions posed in Di Stefano & Kong (2003a). We summarize this progress below.

(1) *What are typical galactic populations of very soft sources?* It is too soon to claim an answer to this question.

We can say, however, the SSSs and QSSs seem to exist in virtually every galaxy. (Ongoing analyses of additional galaxies lend further support to this conclusion.) We have so far carried out only a crude population analysis of the 4 galaxies studied here. In each case though, the data is consistent with a population of at least ~ 500 VSSs with $L > 10^{37}$ erg s $^{-1}$ active at the time of the observation. The true underlying population of such luminous sources could be several times larger. Observations so far provide evidence for galactic populations of low-luminosity VSSs ($L < 10^{37}$ erg s $^{-1}$), but do not constrain its size. With regard to the potential of VSSs to ionize galactic ISMs, we note that even the most conservative estimate of VSS population for these galaxies yields more than 10^{40} erg s $^{-1}$ of highly ionizing radiation released by SSSs in typical galaxies. Although the luminosity is smaller than that associated with young stars, photons from VSSs may dominate at high energies.

(2) *Are any spiral galaxy parameters related to the relative sizes of SSS and QSS populations?* Among the spiral galaxies in this study, there is not enough variation among the values of M_B to allow a search for correlations between M_B and the true size of the SSS/QSS population. The ratio of the number of detected SSSs and QSSs to the total number of detected X-ray sources does vary systematically with inclination (39%, 37%, and 30% for M101, M83, and M51, respectively). If we limit consideration to sources selected by the HR conditions, which seem to be the softest sources selected, the trend appears even stronger (17%, 11%, and 7% for M101, M83, and M51, respectively). This might suggest similar sized populations in each of these galaxies.

(3) *Do elliptical galaxies house large SSS/QSS populations?* The existence of SSSs and QSSs in NGC 4697 demonstrates that there are SSSs in ellipticals. (See also Sarazin, Irwin, & Bregman 2001.) It is difficult to estimate the size of the underlying SSS/QSS populations in galaxies like NGC 4697, largely because we do not yet have good models for the characteristics of the SSS/QSS population in these galaxies. We have demonstrated, however, that, if the sources we detect in NGC 4697 are similar to the SSSs in the Milky Way and Magellanic Clouds that were used to define the class, its population of SSSs is large—about 1250 “classical” SSSs per detected example of a “classical” SSS in NGC 4697. It is possible, however, that many of the 14 detected VSSs are examples of new types of sources. Finally, we note that the data so far are consistent with the hypothesis that a significant portion of the diffuse soft emission found in elliptical galaxies may be due to unresolved SSSs (Fabbiano, Kim, & Trinchieri 1994).

(4) *Within spiral galaxies, what are the relative populations of SSSs/QSSs in the galaxy bulges and disks?* In the 3 spirals we have studied, $f_{SSS+QSS}$, the fraction of SSSs and QSSs located within 1 kpc of the galaxy center is the same as f_{all} , the fraction of all X-ray sources located within 1 kpc of the galaxy center. The values of $f_{SSS+QSS}$ vary significantly among the spiral galaxies, however.

(5) *Do galaxies with massive central black holes have more SSSs/QSSs located within 1 kpc of the nucleus than comparable galaxies without massive central black holes?* To answer this question, we have to rely on the dynamical measurements of the central supermassive BH. M51 is a Seyfert 2 galaxy with a low-luminosity AGN (see, e.g., Ho, Filippenko, & Sar-

gent 1997) and it is very likely that there is a supermassive, $\sim 10^7 M_\odot$ (Hagiwara et al. 2001) BH in the center. M83 might also harbor a $\sim 10^7 M_\odot$ BH (Thatte et al. 2000). The concentration factors for SSSs/QSSs in both M83 and M51 are high, approximately 50 for each galaxy. The concentration factors for all sources in each galaxy is comparable, but somewhat smaller. M101 might have a $< 10^6 M_\odot$ supermassive BH (Moody et al. 1995). The relative values of the concentration factors among the spiral galaxies suggests that the concentration of SSSs/QSSs, and in fact the concentration of all X-ray sources, scales with the mass of the central supermassive BH. It is interesting, but not at this point statistically significant, that the concentration factors are somewhat higher for SSSs/QSSs.

NGC 4697 appears to have the highest-mass central BH of any of the galaxies in our sample ($1.2 \times 10^8 M_\odot$). It is also the galaxy that has the highest concentration factor for all X-ray sources ($\mathcal{F}_{all} = 140$), the highest concentration factor for SSSs ($\mathcal{F}_{SSS+QSS} = 360$), and the largest difference between the central concentration of SSSs and other X-ray sources. From this it seems that interactions near the galaxy center may be playing an important role in creating X-ray sources, and that this is especially true for SSSs/QSSs. (An alternative hypothesis is that the characteristics of the stellar population near the center differ from those elsewhere in the galaxy.) A variety of interactions could enhance the formation of X-ray binaries near the center of the galaxy; it may be that the additional enhancement for SSSs is due to the presence of the cores of stars that have been tidally disrupted by the central BH.

(6) *For all galaxies, are the positions of SSSs and QSSs correlated to the positions of other objects, such as HII regions, planetary nebulae, supernova remnants, or globular clusters?* In the 3 spiral galaxies we have studied, the SSSs seem to be concentrated in the spiral arms. Ongoing work on SSSs and QSSs in M101 indicates that they may be preferentially located near HII regions and SNRs, suggesting that some SSSs/QSSs in M101 may be related to young populations.

(7) *Are SSSs significant contributors to the rates of Type Ia SNe?* It is too soon to say. To use the data to answer this question, we need to estimate the fraction of the SSSs in each galaxy that are accreting WDs. This is difficult to do, even in the Magellanic Clouds. There are, however, some signatures which can help. First, the WD models developed to date invoke donor stars that too old to be concentrated in the spiral arms; the fraction of sources located away from the spiral arms and from regions with recent star formation can provide clues about the size of the NBWD population. Second, some of the accreting WDs that may be Type Ia progenitors should be surrounded by large, distinctive ionization nebulae (Di Stefano 1996).⁷ In nearby galaxies where optical counterparts can be identified, we may be able to detect some of the distinctive disk features of close binary SSSs ($P_{orb} < 3$ days) or to detect the donor stars in wide binary SSSs (P_{orb} generally is more than 100 days).

4.1. New Questions

(8) *What are the ultraluminous SSSs?* A natural suggestion is that they are BHs. In fact, if there are BHs with masses filling the gap between the $\sim 10 M_\odot$ BHs thought to be stellar remnants, and the $> 10^6 M_\odot$ BHs found at the centers of galax-

⁷ The reasons are the following. (1) SSSs emit enough photons to ionize large (> 10 pc) regions of the surrounding ISM, if the number density in their surroundings is moderate, on the order of 1 atom cm $^{-3}$ (Rappaport, Kallman, & Malina 1994). (2) These nebulae have distinctive optical emission signatures that can be significantly different from other nebulae, such as PNe and SNRs (Rappaport & Chiang 1996; Di Stefano Paerels, & Rappaport 1996). (3) These nebulae could be detectable for much of the lifetime of the SSS state ($\sim 10^7$ yrs), as long as the duty cycle is $> \sim 1\%$ (Chiang & Rappaport 1996).

ies, then SSS behavior is predicted for a wide range of masses, source luminosities, and efficiency factors. If BHs with masses in this intermediate range do not exist, or are not found in binaries, then the explanation of ultraluminous SSSs may be more complicated.

(9) *What are the low-luminosity high-temperature VSSs?* The data provide a hint of a population of sources with temperatures near or over 100 eV, but with luminosities between 10^{36} erg s $^{-1}$ and 10^{37} erg s $^{-1}$. NBWDs at this temperature are generally expected to be more luminous. If evidence for this high-T/low-L SSS population is found in other investigations, a new model for some SSSs will be required. At present, there is no “canonical” model for QSSs. Intermediate-mass BHs provide one possible explanation. Consider, e.g., a 200 eV source with $L_X \sim 5 \times 10^{37}$ erg s $^{-1}$. This could correspond to a BH of roughly $50 M_\odot$ accreting at a rate of roughly 1% \dot{m}_{Edd} . (Note that if the bolometric luminosities were significantly smaller, the source might not be expected to be in the soft state.)

(10) *Is there a significant population of quasisoft sources and, if so, what is the nature of the sources?* Some of the SSSs and QSSs may be SNRs. If so, we expect the flux we measure in observations taken during the next few years to be comparable to the values already measured; some may be associated in optical nebulae. It will be important to search for quasisoft sources that are not SNRs.

(11) *If a subset of VSSs are young ($< 10^8$ yrs), what are they?* Some of them may be SNRs, but we have argued (§5.4.2) that the majority of them are not SNRs. Some may be BHs, some may be neutron stars, perhaps analogs of RX J0059.2-7138. It is even possible that some may be NBWDs. One scenario we propose (R. Di Stefano, in preparation) is one in which a primordial binary with 2 relatively massive stars ($> 3 M_\odot$) evolves into a binary with a massive WD in orbit with a massive star. Even if the primary never fills its Roche lobe, the system could become a symbiotic which experiences an SSS phase. If the primary *will* fill its Roche lobe, an epoch of irradiation-driven

winds prior to contact could also lead to SSS behavior. Finally, in some of these wind-driven systems, the primary mass may be decreased enough that mass transfer is not dynamically unstable when contact is established, and the SSS behavior can continue.

4.2. Prospects

Chandra observations are beginning to help us answer key questions about SSSs and to demonstrate that there are new horizons in SSS research. An unanticipated result of this research is the discovery that galaxies contain a significant number of X-ray sources that appear to be hotter than the canonical SSSs that established the class. Discovering the nature of these QSSs presents a fresh challenge. Continuing observations with both *Chandra* and *XMM* should lead to important results. With the publication of this paper we will make our code available to other researchers, and hope that it can facilitate comparative studies of the VSS populations of different galaxies.

We are grateful to Pauline Barmby, Mike Garcia, Jochen Greiner, Roy Kilgard, Miriam Krauss, Jeff McClintock, Koji Mukai, Paul Plucinsky, Will Pence, Andrea Prestwich, Frank Primini, Roberto Soria, Douglas Swartz, Harvey Tananbaum, Ben Williams, Kinwah Wu, and Andreas Zezas for stimulating discussions and comments. We are grateful to Paul Green and the ChaMP collaboration for providing blank field source data. This research has made use of the electronic catalog of supersoft X-ray sources available at URL <http://www.mpe.mpg.de/~jcg/sssscat.html> and maintained by J. Greiner. RD would like to thank the Aspen Center for Physics for providing a stimulating environment, and the participants of the 2002 workshop on *Compact Object Populations in External Galaxies* for insightful comments. AKHK acknowledges support from the Croucher Foundation. This work was supported by NASA under AR1-2005B, GO1-2022X, and an LTSA grant, NAG5-10705.

REFERENCES

Chiang, E. & Rappaport, S. 1996, *ApJ*, 469, 255
 Di Stefano, R., Greiner, J., Murray, S., Garcia, M. 2001, *ApJ*, 51L, 37
 Di Stefano, R. & Kong, A. K. H. 2003a, *ApJ*, 592, 884
 Di Stefano, R. & Kong, A. K. H. 2003b, *ApJ*, submitted (astro-ph/0311374)
 Di Stefano, R. et al. 2003, *ApJ*, submitted (astro-ph/0306440)
 Di Stefano, R. 1996, in *Supersoft X-Ray Sources*, Proceedings of the International Workshop Held in Garching, Germany, 28 February - 1 March 1996. Lecture Notes in Physics, Vol. 472, edited by Jochen Greiner. Springer-Verlag, Berlin Heidelberg New York, 1996., p.193
 Di Stefano, R., Paerels, F., & Rappaport, S. 1995, *ApJ*, 450, 705
 Di Stefano, R., Rappaport, S. 1994, *ApJ*, 437, 733
 Fabbiano, G., Kim, D.-W., Trinchieri, G. 1994, *ApJ*, 428, 555
 Faber, S.M., Wegner, G., Burstein, D., Davies, R.L., Dressler, A., Lynden-Bell, D., Terlevich, R. J. 1989, *ApJS*, 71, 173
 Feldmeier, J.J., Ciardullo, R., Jacoby, G.H. 1997, *ApJ*, 479, 231
 Freedman, W.L., et al. 2001, *ApJ*, 553, 47
 Greiner J. 2000 *New Astronomy* 5, 137.
 Greiner, J., Tovmessian, G.H., Di Stefano, R., Prestwich, A., Gonzalez-Riestra, R., Szentasko, L., & Chevarria, C. 1999, *A&A*, 343, 183
 Greiner, J. & van Teeseling 1998, *A&A*, 339L, 21
 Hagiwara, Y., Henkel, C., Menten, K.M., Nakai, N. 2001 *ApJ*, 560, L37
 Ho, L. C., Filippenko, A. C., & Sargent, W. L. W. 1997, *ApJS*, 112, 315
 Ho, L.C. 2002, *ApJ*, 564, 120
 Kenyon, S.J. 1986, *The Symbiotic Stars*, CUP
 Karachentsev, I.D., et al. 2002, *A&A*, 385, 21
 Kong, A.K.H., Garcia, M.R., Primini, F.A., & Murray, S.S. 2002, *ApJ*, 580, L125
 Kong, A. K. H., Sjouwerman, L. O., Williams, B. F., Garcia, M. R., & Dickel, J. R. 2003, *ApJ*, 590, L21
 Kong, A.K.H., & Di Stefano, R. 2003, *ApJ*, 590, L13
 Kong, A.K.H., & Di Stefano, R. 2004, *ATel*, 222
 Long, K.S., Helfand, D.J., & Grabelsky, D.A. 1981, *ApJ*, 248, 925
 Matonick, D.M., & Fesen, R.A. 1997, *ApJS*, 112, 49
 Moody, J. W., Roming, P.W.A., Joner, M.D., Hintz, E.G., Geisler, D., Durrell, P.R., Scowen, P.A., Jee, R.O. 1995, *AJ*, 110, 2088
 Mukai, K., Pence, W.D., Snowden S.L., & Kuntz, K.D. 2002, *ApJ*, 582, 184
 Nedialkov, P., Orio, M., Birkle, K., Conselice, C., Della Valle, M., Greiner, J., Magnier, E., & Tikhonov, N. A. 2002, *A&A*, 389, 439
 Patterson, J., Thorstensen, J. R., Fried, R., Skillman, D. R., Cook, L. M., & Jensen, L. 2001, *PASP*, 113, 72
 Pence, W. D., Snowden, S. L., Mukai, K., & Kuntz, K. D. 2001, *ApJ*, 561, 189
 Rappaport, S., Chiang, E., Kallman, T., & Malina, R. 1994, *ApJ*, 431, 237
 Rappaport, S., Di Stefano, R., Smith, J.D. 1994, *ApJ*, 426, 692
 Sarazin, Craig L., Irwin, Jimmy A., Bregman, Joel N. 2001, *ApJ*, 556, 533
 Scowen P.A., Dufour R.J., & Hester J.J. 1992, *AJ*, 104, 92
 Soria, R. & Wu, K. 2002, *A&A*, 384, 99
 Soria, R. & Wu, K. 2003, *A&A*, 410, 53
 Swartz, D.A., Ghosh, K.K., Suleimanov, V., Tennant, A.F., & Wu, K. 2002, *ApJ*, 574, 382
 Terashima, Y. & Wilson, A.S. 2003, *ApJ*, 601, 735
 Thatte, N., Tecza, M., & Genzel, R. 2000, *A&A*, 364, L47
 Tonry, J.L., Dressler, A., Blakeslee, J.P., Ajhar, E.A., Fletcher, A.B., Luppino, G.A., Metzger, M.R., Moore, C.B. 2001, *ApJ*, 546, 681
 Tully, R.B. 1988, in *Nearby Galaxies Catalog*, Cambridge and New York, Cambridge University Press,
 Vanlandingham, K. M., Starrfield, S., Shore, S. N., & Sonneborn, G. 1999, *MNRAS*, 308, 577

TABLE 1
SUMMARY OF SAMPLE GALAXIES

Name	Type	Distance (Mpc)	D_{25} (arcmin)	M_B	Inclination	N_H (10^{20} cm^{-2})	<i>Chandra</i> exposure (ks)	$\log(M_{HI})$ (M_\odot)	M_{BH} ($\times 10^9 M_\odot$)	N_{VSS}/N_{total} ^a
M101	Sc	5.4, 6.7 ¹	23.8	-20.45	0 ^o	1.2	94.4	10.05	< 0.01 ²	53/118
M83	Sc	4.7, 4.57 ³	11.5	-20.31	24 ^o	3.8	49.5	10.01	0.1 ⁴	54/127
M51	Sc ^b	7.7, 8.4 ⁵	13.6	-20.75	64 ^o	1.6	14.9	9.46	0.1 ⁶	23/72
NGC 4697	E	23.3, 15.9 ⁷ , 11.7 ⁸	7.1	-21.67	44 ^o ^c	2.1	39.3	0.53	1.2 ⁹	19/91

Note. — All data are from Nearby Galaxies Catalogue (Tully 1988) unless specified.

^aRatio of number of VSSs to total number of X-ray sources.

^bSeyfert 2 galaxy.

^cFor elliptical galaxies the inclination is given by $3^o + \arccos\left(\sqrt{(d/D)^2 - 0.2^2}/(1 - 0.2^2)\right)$, where d/D is the axial ratio of minor to major diameter (Tully 1988). This inclination angle is generally unrelated to the value of N_H .

References. — 1: Freedman et al. 2001; 2: Moody et al. 1995; 3: Karachentsev et al. 2002; 4: Thatte et al. 2000; 5: Feldmeier et al. 1997; 6: Hagiwara et al. 2001; 7: Faber et al. 1989; 8: Tonry et al. 2001; 9: Ho 2002

TABLE 2
SSS AND QSS SOURCE LIST OF M101

Object	R.A.	Dec.	Soft		Medium		Hard		HR1 ^a	HR2 ^b	Note ^c
			(h:m:s)	($^{\circ}$; ' ; '')	Counts	S/N	Counts	S/N			
SSS-HR											
M101-15(10)	14:02:59.4	+54:20:42	31.3	5.3	1.3	0.6	0.0	0.0	-0.9(-0.8)	-1.0(-0.9)	
M101-18(13*)	14:03:01.1	+54:23:41	169.6	12.9	0.0	0.0	0.1	0.1	-1.0(-1.0)	-1.0(-1.0)	
M101-21(16*)	14:03:02.5	+54:24:16	74.2	8.3	0.0	0.0	0.0	0.0	-1.0(-0.9)	-1.0(-1.0)	
M101-34(27)	14:03:07.9	+54:21:23	35.7	5.8	1.8	0.8	0.0	0.0	-0.9(-0.8)	-1.0(-0.9)	
M101-37(30*)	14:03:08.5	+54:20:57	29.3	5.0	1.0	0.4	0.4	0.0	-0.9(-0.8)	-1.0(-0.9)	
M101-38(31)	14:03:08.6	+54:23:36	20.7	4.1	0.0	0.0	0.0	0.0	-1.0(-0.9)	-1.0(-1.0)	
M101-43(36)	14:03:10.6	+54:21:26	18.2	3.8	0.0	0.0	0.0	0.0	-1.0(-1.0)	-1.0(-0.9)	
M101-50(43)	14:03:13.2	+54:21:57	31.3	5.3	0.0	0.0	0.0	0.1	-1.0(-1.0)	-1.0(-0.8)	SNR
M101-51(45*)	14:03:13.6	+54:20:09	219.1	14.6	0.3	0.1	0.0	0.0	-1.0(-1.0)	-1.0(-1.0)	HII
M101-55(48)	14:03:13.9	+54:18:11	34.3	5.6	1.4	0.6	0.0	0.0	-0.9(-0.8)	-1.0(-0.9)	
M101-78(73)	14:03:22.6	+54:20:38	34.3	5.4	1.5	0.6	1.0	0.4	-0.9(-0.8)	-1.0(-0.8)	HII
M101-80(75)	14:03:24.0	+54:23:37	68.7	8.0	0.8	0.3	0.0	0.0	-1.0(-0.9)	-1.0(-0.9)	HII
M101-97(92)	14:03:29.8	+54:20:58	71.9	7.9	0.0	0.0	0.0	0.0	-1.0(-0.9)	-1.0(-0.9)	
M101-101(96*)	14:03:31.9	+54:23:23	30.9	5.1	0.0	0.0	0.0	0.0	-1.0(-0.9)	-1.0(-0.9)	
M101-102(98)	14:03:32.3	+54:21:03	8512.0	92.2	658.4	25.6	68.0	8.0	-0.9(-0.9)	-1.0(-1.0)	
M101-104(99*)	14:03:33.3	+54:18:00	227.8	14.6	0.3	0.1	1.1	0.3	-1.0(-1.0)	-1.0(-1.0)	HII
SSS-3σ											
M101-5	14:02:51.7	+54:19:33	13.0	3.2	1.7	0.8	0.0	0.0	-0.8(-0.6)	-1.0(-0.7)	SNR
M101-11(8*)	14:02:57.0	+54:19:48	34.2	5.6	0.0	0.0	2.5	1.0	-1.0(-0.9)	-0.9(-0.8)	
M101-16(11)	14:03:00.5	+54:20:02	31.9	5.2	0.0	0.0	4.2	1.5	-1.0(-0.9)	-0.8(-0.7)	SNR, HII
M101-17(12)	14:03:00.8	+54:20:17	17.1	3.5	0.0	0.0	2.8	1.1	-1.0(-0.8)	-0.7(-0.6)	
M101-24	14:03:04.6	+54:20:37	15.3	3.5	0.0	0.0	0.0	0.0	-1.0(-0.8)	-1.0(-0.8)	
M101-27(20)	14:03:05.2	+54:23:11	19.0	4.0	1.7	0.7	0.8	0.3	-0.8(-0.7)	-0.9(-0.8)	
M101-49(42)	14:03:12.8	+54:19:01	18.6	4.0	0.5	0.2	2.6	1.0	-1.0(-0.8)	-0.8(-0.6)	SNR, HII
M101-57(52)	14:03:14.6	+54:21:52	17.9	3.8	1.9	0.8	0.0	0.0	-0.8(-0.7)	-1.0(-0.8)	SNR
M101-60(55)	14:03:15.0	+54:20:18	18.0	3.7	0.0	0.0	0.5	0.2	-1.0(-0.8)	-1.0(-0.8)	
M101-72(68)	14:03:21.1	+54:19:08	21.2	4.2	1.7	0.7	0.0	0.0	-0.9(-0.7)	-1.0(-0.8)	
M101-76(72*)	14:03:21.7	+54:20:24	19.4	3.7	0.6	0.2	0.0	0.0	-0.9(-0.8)	-1.0(-0.8)	HII
M101-85(80*)	14:03:25.3	+54:21:13	27.3	4.7	0.0	0.0	3.6	1.3	-1.0(-0.9)	-0.8(-0.7)	HII
M101-86(81)	14:03:25.8	+54:21:25	18.6	3.6	0.7	0.3	0.0	0.0	-1.0(-0.8)	-1.0(-1.0)	SNR, HII
M101-88(84)	14:03:26.6	+54:20:43	45.8	6.1	4.3	1.7	5.3	1.9	-0.8(-0.8)	-0.8(-0.7)	SNR, HII
M101-92	14:03:27.9	+54:18:45	27.1	4.2	3.5	1.3	3.5	1.1	-0.8(-0.7)	-0.8(-0.7)	HII
M101-95(90)	14:03:28.8	+54:20:59	24.6	4.4	3.1	1.3	0.3	0.1	-0.8(-0.7)	-1.0(-0.8)	
QSS-NOH											
M101-77	14:03:21.7	+54:22:32	9.4	2.5	0.7	0.3	0.5	0.2	-0.9(-0.6)	-0.9(-0.6)	PN
M101-93(88)	14:03:28.6	+54:22:02	12.8	3.0	1.1	0.4	1.3	0.5	-0.9(-0.7)	-0.8(-0.6)	
M101-106(101*)	14:03:33.9	+54:20:11	23.1	3.7	3.9	1.4	0.0	0.0	-0.7(-0.6)	-1.0(-0.8)	SNR, HII
QSS-SNOH											
M101-2(1)	14:02:49.1	+54:18:42	15.4	3.1	8.7	2.7	0.0	0.0	-0.3(-0.3)	-1.0(-0.8)	HII
M101-25(18)	14:03:04.7	+54:19:25	16.0	3.3	4.3	1.7	1.4	0.5	-0.6(-0.5)	-0.8(-0.7)	HII
M101-61(56)	14:03:15.5	+54:17:04	53.7	6.4	9.8	2.7	0.0	0.0	-0.7(-0.7)	-1.0(-0.9)	HII
QSS-HR₁											
M101-3(2)	14:02:49.6	+54:19:59	19.4	4.1	6.4	2.3	1.8	0.7	-0.5(-0.5)	-0.8(-0.7)	
M101-96(91)	14:03:28.9	+54:21:49	13.3	3.1	4.7	1.8	1.9	0.7	-0.5(-0.4)	-0.8(-0.6)	HII
QSS-3σ_1											
M101-6(4)	14:02:52.1	+54:19:47	12.5	2.9	0.4	0.2	2.3	0.9	-0.9(-0.7)	-0.7(-0.6)	
M101-12	14:02:57.1	+54:22:33	9.6	2.5	0.0	0.0	0.8	-1.0(-0.7)	-0.7(-0.5)		
M101-48(41)	14:03:12.7	+54:17:44	11.6	2.7	7.1	2.4	2.4	0.9	-0.2(-0.2)	-0.7(-0.5)	SNR
M101-58(53)	14:03:14.8	+54:21:10	13.6	2.9	5.2	1.9	2.0	0.9	-0.5(-0.4)	-0.8(-0.6)	
M101-59(54)	14:03:14.8	+54:21:23	11.2	2.9	4.9	2.0	1.7	0.7	-0.4(-0.3)	-0.7(-0.6)	
M101-87(82)	14:03:26.2	+54:19:51	11.6	2.9	0.5	0.2	1.5	0.6	-0.9(-0.7)	-0.8(-0.6)	HII
QSS-σ											
M101-53(45*)	14:03:13.6	+54:19:09	76.3	8.4	36.3	5.9	3.9	1.4	-0.4(-0.3)	-0.9(-0.9)	HII
QSS-FNOH											
M101-1	14:02:48.8	+54:20:34	11.9	3.0	3.0	1.3	0.0	0.0	-0.6(-0.5)	-1.0(-0.8)	
M101-8(6)	14:02:53.2	+54:18:55	5.7	1.7	9.9	3.0	1.2	0.5	0.3(0.2)	-0.7(-0.4)	
M101-19(14)	14:03:01.3	+54:21:33	10.2	2.8	5.7	2.2	0.9	0.4	-0.3(-0.3)	-0.8(-0.6)	
M101-112	14:03:39.0	+54:16:56	17.3	0.6	19.6	3.7	0.0	0.0	0.1(-0.3)	-1.0(-0.7)	
QSS-MNOH											
M101-114(107)	14:03:41.3	+54:19:04	280.1	14.5	64.4	7.2	1.4	0.3	-0.6(-0.6)	-1.0(-1.0)	
M101-116(109)	14:03:51.9	+54:21:49	99.8	8.7	15.3	3.2	0.0	0.0	-0.7(-0.7)	-1.0(-0.9)	HII

Note. — The object ID in parentheses is from Pence et al. (2001); SSSs selected by Pence et al. (2001) are noted by “*”.

^a(M-S)/(M+S); value in parentheses is the maximum of HR1.

^b(H-S)/(H+S); value in parentheses is the maximum of HR2.

^cEntries indicate that an object of the type listed is within 10'' of a VSS; SNR: SNR catalog (94 objects in total) from Matonick & Fesen (1997); HII: HII region catalog (248 objects in total) Scowen et al. (1992); PN: PN catalog (65 objects in total) from Feldmeier et al. (1997)

TABLE 3
SSS AND QSS SOURCE LIST OF M83

Object	R.A. (h:m:s)	Dec. ($^{\circ}$: ' : '')	Soft		Medium		Hard		HR1 ^a	HR2 ^b
			Counts	S/N	Counts	S/N	Counts	S/N		
SSS-HR										
M83-20	13:36:53.9	-29:48:48	43.0	5.7	2.7	1.1	2.6	0.9	-0.9(-0.8)	-0.9(-0.8)
M83-42	13:36:59.1	-29:53:36	30.5	5.3	0.0	0.0	0.0	0.0	-1.0(-0.9)	-1.0(-0.9)
M83-50	13:37:00.4	-29:50:54	105.1	10.0	0.8	0.3	0.0	0.0	-1.0(-0.9)	-1.0(-1.0)
M83-54	13:37:01.1	-29:54:49	132.6	11.4	1.8	0.8	0.7	0.3	-1.0(-1.0)	-1.0(-1.0)
M83-79	13:37:06.1	-29:52:32	108.6	10.3	1.8	0.9	0.0	0.0	-1.0(-0.9)	-1.0(-1.0)
M83-81	13:37:06.5	-29:54:16	15.7	3.7	0.0	0.0	0.0	0.0	-1.0(-0.8)	-1.0(-0.8)
M83-88	13:37:07.4	-29:51:33	17.5	3.8	0.0	0.0	0.0	0.0	-1.0(-0.8)	-1.0(-0.8)
M83-98	13:37:12.8	-29:50:12	35.9	5.8	2.1	1.0	1.6	0.7	-0.9(-0.8)	-0.9(-0.8)
M83-111	13:36:59.5	-29:52:03	78.2	8.4	5.9	2.2	2.0	0.9	-0.9(-0.8)	-1.0(-0.9)
M83-128	13:36:57.7	-29:53:53	29.6	5.2	1.6	0.7	0.0	0.0	-0.9(-0.8)	-1.0(-0.8)
SSS-3σ										
M83-1	13:36:40.8	-29:51:18	25.2	4.7	2.9	1.3	1.6	0.6	-0.8(-0.7)	-0.9(-0.8)
M83-7	13:36:48.2	-29:52:44	13.1	3.3	1.9	0.9	1.6	0.7	-0.8(-0.6)	-0.8(-0.6)
M83-10	13:36:49.8	-29:52:17	29.3	5.0	2.7	1.2	2.4	1.0	-0.8(-0.8)	-0.8(-0.8)
M83-19	13:36:53.6	-29:56:00	24.7	4.8	2.3	1.1	2.8	1.2	-0.8(-0.7)	-0.8(-0.7)
M83-25	13:36:55.0	-29:52:39	27.5	5.0	3.3	1.8	0.0	0.0	-0.8(-0.7)	-1.0(-0.9)
M83-41	13:36:58.7	-29:51:00	15.2	3.5	0.4	0.1	0.0	0.0	-1.0(-0.7)	-1.0(-0.8)
M83-46	13:36:59.8	-29:55:25	28.0	5.1	0.8	0.3	2.1	0.9	-1.0(-0.8)	-0.9(-0.8)
M83-48	13:37:00.0	-29:54:17	11.5	3.0	0.9	0.4	0.0	0.0	-0.9(-0.6)	-1.0(-0.8)
M83-53	13:37:01.0	-29:50:56	18.4	3.7	1.2	0.5	0.0	0.0	-0.9(-0.7)	-1.0(-0.8)
M83-60	13:37:01.7	-29:51:13	22.7	4.2	3.3	1.4	0.3	0.1	-0.7(-0.7)	-1.0(-0.8)
M83-73	13:37:04.5	-29:51:08	14.0	3.1	0.0	0.0	0.0	0.0	-1.0(-0.8)	-1.0(-0.8)
M83-80	13:37:06.1	-29:54:44	39.6	6.2	5.0	2.0	0.0	0.0	-0.8(-0.7)	-1.0(-0.9)
M83-91	13:37:08.3	-29:51:26	20.8	4.1	0.2	0.1	0.8	0.3	-1.0(-0.8)	-0.9(-0.8)
M83-92	13:37:08.5	-29:51:35	12.8	3.0	0.0	0.0	0.0	0.0	-1.0(-1.0)	-1.0(-1.0)
M83-93	13:37:11.8	-29:52:15	45.0	6.5	4.6	1.8	1.3	0.6	-0.8(-0.7)	-0.9(-0.9)
M83-94	13:37:12.1	-29:50:56	14.2	3.4	0.6	0.2	0.6	1.0	-0.9(-0.7)	-0.7(-0.6)
M83-97	13:37:12.7	-29:52:00	14.8	3.5	0.0	0.0	0.6	0.3	-1.0(-0.8)	-0.9(-0.7)
M83-127	13:37:01.6	-29:52:01	32.9	5.2	3.1	1.3	1.0	0.4	-0.8(-0.8)	-0.9(-0.9)
QSS-NOH										
M83-12	13:36:50.9	-29:52:26	12.0	2.8	3.7	1.6	0.0	0.0	-0.5(-0.5)	-1.0(-0.8)
M83-22	13:36:54.1	-29:52:09	10.2	2.9	2.9	1.3	0.0	0.0	-0.6(-0.5)	-1.0(-0.7)
M83-43	13:36:59.3	-29:55:08	9.7	2.7	2.2	1.0	0.8	0.3	-0.6(-0.5)	-0.9(-0.6)
M83-58	13:37:01.6	-29:54:10	10.1	2.8	2.9	1.3	0.0	0.0	-0.6(-0.5)	-1.0(-0.7)
M83-85	13:37:07.0	-29:53:20	6.6	2.2	1.0	0.4	0.0	0.0	-0.8(-0.5)	-1.0(-0.7)
M83-86	13:37:07.1	-29:52:02	15.8	3.7	3.2	1.4	0.0	0.0	-0.7(-0.6)	-1.0(-0.8)
QSS-SNOH										
M83-15	13:36:52.8	-29:52:31	20.0	3.9	7.5	2.5	0.0	0.0	-0.5(-0.4)	-1.0(-0.8)
M83-24	13:36:55.0	-29:53:04	21.2	4.0	7.8	2.6	0.0	0.0	-0.5(-0.4)	-1.0(-0.9)
QSS-HR₁										
M83-11	13:36:50.8	-29:52:40	20.3	3.8	7.5	2.5	1.7	0.7	-0.5(-0.4)	-0.9(-0.7)
M83-13	13:36:51.1	-29:50:43	25.0	4.2	9.6	2.9	1.9	0.8	-0.5(-0.4)	-0.9(-0.8)
M83-17	13:36:53.1	-29:53:25	33.8	5.3	5.1	1.9	1.8	0.8	-0.7(-0.7)	-0.9(-0.8)
M83-18	13:36:53.2	-29:52:42	27.9	4.5	11.8	3.3	1.4	0.6	-0.4(-0.4)	-0.9(-0.8)
M83-64	13:37:02.4	-29:51:26	64.8	7.6	10.6	3.1	1.4	0.6	-0.7(-0.7)	-1.0(-0.9)
M83-106	13:37:17.4	-29:51:54	13.8	3.5	5.0	2.0	1.7	0.7	-0.5(-0.4)	-0.8(-0.6)
M83-114	13:37:00.2	-29:52:06	80.1	8.9	10.3	3.1	2.0	0.9	-0.8(-0.7)	-0.9(-0.8)
M83-120	13:37:00.6	-29:52:04	356.5	18.8	61.1	7.8	1.6	0.7	-0.7(-0.7)	-1.0(-1.0)
QSS-3σ_1										
M83-89	13:37:07.5	-29:48:59	11.5	2.2	2.0	0.8	1.4	0.6	-0.7(-0.6)	-0.8(-0.6)
M83-90	13:37:08.2	-29:49:16	10.3	2.3	2.0	0.8	1.5	0.6	-0.7(-0.5)	-0.8(-0.6)
QSS-σ										
M83-105	13:37:17.2	-29:51:53	66.1	8.1	22.5	4.7	3.9	1.7	-0.5(-0.5)	-0.9(-0.8)
M83-116	13:37:00.4	-29:51:59	682.2	26.0	140.1	11.8	16.4	4.0	-0.7(-0.7)	-1.0(-0.9)
M83-117	13:37:00.5	-29:51:56	780.3	27.9	207.9	14.4	24.7	4.9	-0.6(-0.6)	-0.9(-0.9)
M83-119	13:37:00.6	-29:51:59	526.6	22.9	110.4	10.5	10.0	3.0	-0.7(-0.6)	-1.0(-1.0)
QSS-FNOH										
M83-66	13:37:03.0	-29:49:45	11.5	2.5	4.0	1.6	0.0	0.0	-0.5(-0.4)	-1.0(-0.8)
QSS-MNOH										
M83-35	13:36:57.8	-29:53:03	68.6	8.1	13.1	3.5	0.0	0.0	-0.7(-0.6)	-1.0(-0.9)
M83-78	13:37:06.0	-29:55:14	56.7	7.4	13.4	3.6	0.6	0.2	-0.6(-0.6)	-1.0(-0.9)
M83-115	13:37:00.3	-29:52:05	86.4	9.2	12.4	3.5	0.9	0.4	-0.8(-0.7)	-1.0(-0.9)

^a(M-S)/(M+S); value in parentheses is the maximum of HR1.

^b(H-S)/(H+S); value in parentheses is the maximum of HR2.

TABLE 4
SSS AND QSS SOURCE LIST OF M51

Object	R.A. (h:m:s)	Dec. ($^{\circ}$: ' : '')	Soft		Medium		Hard		HR1 ^a	HR2 ^b
			Counts	S/N	Counts	S/N	Counts	S/N		
SSS-HR										
M51-12	13:29:43.3	+47:11:34	272.7	16.5	5.2	2.1	1.0	0.4	-1.0(-0.9)	-1.0(-1.0)
M51-42	13:29:55.4	+47:11:43	14.7	3.6	0.0	0.0	0.0	0.0	-1.0(-0.8)	-1.0(-0.8)
M51-58	13:30:02.3	+47:12:38	20.4	4.5	0.0	0.0	0.0	0.0	-1.0(-0.9)	-1.0(-0.9)
SSS-3σ										
M51-14	13:29:44.0	+47:11:56	7.9	2.6	0.0	0.0	0.9	0.4	-1.0(-0.7)	-0.8(-0.5)
M51-17	13:29:45.9	+47:10:55	11.9	3.3	0.0	0.0	0.0	0.0	-1.0(-0.8)	-1.0(-0.8)
M51-22	13:29:50.1	+47:14:20	8.7	2.8	0.0	0.0	0.0	0.0	-1.0(-0.7)	-1.0(-0.7)
M51-27	13:29:52.0	+47:12:13	9.9	2.9	0.0	0.0	1.0	0.4	-1.0(-0.7)	-0.8(-0.6)
M51-41	13:29:55.1	+47:10:42	8.1	2.6	0.0	0.0	0.8	0.4	-1.0(-0.7)	-0.8(-0.5)
M51-43	13:29:55.4	+47:14:02	10.6	3.0	0.0	0.0	0.9	0.4	-1.0(-0.8)	-0.8(-0.6)
M51-45	13:29:56.0	+47:13:51	7.7	2.4	1.0	0.4	0.7	0.3	-0.8(-0.5)	-0.8(-0.5)
M51-59	13:30:04.1	+47:10:03	10.2	3.1	2.1	1.0	0.8	0.3	-0.7(-0.5)	-0.9(-0.6)
M51-62	13:30:05.7	+47:10:31	8.2	2.7	0.9	0.4	0.0	0.0	-0.8(-0.5)	-1.0(-0.7)
M51-64	13:30:06.0	+47:14:04	9.8	3.0	1.9	0.9	0.5	0.2	-0.7(-0.5)	-0.9(-0.6)
QSS-NOH										
M51-23	13:29:50.3	+47:13:22	4.7	1.9	1.0	0.4	0.0	0.0	-0.6(-0.4)	-1.0(-0.6)
M51-70	13:30:20.9	+47:13:53	5.2	1.9	3.4	1.4	0.9	0.3	-0.2(-0.2)	-0.7(-0.4)
QSS-SNOH										
M51-6	13:29:38.6	+47:13:36	20.7	4.5	5.3	2.1	1.1	0.5	-0.6(-0.5)	-0.9(-0.8)
M51-37	13:29:54.3	+47:11:21	10.9	3.0	2.1	1.0	0.0	0.0	-0.7(-0.5)	-1.0(-0.8)
M51-44	13:29:55.8	+47:11:44	12.2	3.2	3.1	1.4	0.0	0.0	-0.6(-0.5)	-1.0(-0.8)
QSS-HR₁										
M51-60	13:30:04.5	+47:10:31	11.2	3.3	6.1	2.3	2.0	0.9	-0.3(-0.2)	-0.7(-0.6)
QSS-σ										
M51-10	13:29:39.9	+47:12:36	201.9	14.2	70.4	8.4	9.2	2.9	-0.5(-0.5)	-0.9(-0.9)
QSS-FNOH										
M51-5	13:29:38.1	+47:16:12	51.7	7.1	10.8	3.2	0.0	0.0	-0.7(-0.6)	-1.0(-0.9)
M51-32	13:29:53.5	+47:11:26	9.8	2.6	3.1	1.4	0.9	0.4	-0.5(-0.4)	-0.8(-0.6)
M51-57	13:30:02.1	+47:12:38	9.1	2.9	4.1	1.8	0.0	0.0	-0.4(-0.3)	-1.0(-0.7)

^a(M-S)/(M+S); value in parentheses is the maximum of HR1.

^b(H-S)/(H+S); value in parentheses is the maximum of HR2.

TABLE 5
SSS AND QSS SOURCE LIST OF NGC4697

Object	R.A. (h:m:s)	Dec. ($^{\circ}$: ' : '')	Soft		Medium		Hard		HR1 ^a	HR2 ^b
			Counts	S/N	Counts	S/N	Counts	S/N		
SSS-HR										
NGC4697-16	12:48:37.1	-05:47:58	63.0	7.9	0.0	0.0	0.0	0.0	-1.0(-1.0)	-1.0(-0.9)
NGC4697-19	12:48:34.5	-05:47:49	73.7	8.5	0.9	0.4	0.0	0.0	-1.0(-0.9)	-1.0(-1.0)
NGC4697-52	12:48:41.2	-05:48:19	58.6	7.5	0.0	0.0	0.7	0.3	-1.0(-0.9)	-1.0(-0.9)
SSS-3σ										
NGC4697-91	12:48:38.9	-05:47:31	12.7	3.5	0.0	0.0	0.0	0.0	-1.0(-0.8)	-1.0(-0.8)
QSS-NOH										
NGC4697-73	12:48:24.1	-05:48:16	17.3	4.0	3.6	1.6	0.2	0.0	-0.7(-0.6)	-1.0(-0.8)
NGC4697-86	12:48:19.6	-05:47:33	8.2	2.6	3.1	1.4	0.4	0.2	-0.5(-0.4)	-0.9(-0.6)
QSS-SNOH										
NGC4697-2	12:48:36.0	-05:48:03	15.7	3.9	8.4	2.8	0.9	0.4	-0.3(-0.3)	-0.9(-0.7)
NGC4697-9	12:48:35.4	-05:47:54	40.2	6.2	7.0	2.5	0.0	0.0	-0.7(-0.7)	-1.0(-0.9)
NGC4697-10	12:48:36.5	-05:48:01	11.5	3.3	6.3	2.4	0.0	0.0	-0.3(-0.3)	-1.0(-0.8)
NGC4697-17	12:48:37.0	-05:47:53	13.6	3.5	6.2	2.3	0.5	0.2	-0.4(-0.3)	-0.9(-0.7)
QSS-HR₁										
NGC4697-13	12:48:36.2	-05:48:15	12.5	3.1	4.1	1.7	1.3	0.5	-0.5(-0.4)	-0.8(-0.6)
NGC4697-29	12:48:33.3	-05:48:02	15.3	3.7	6.8	2.4	1.8	0.8	-0.4(-0.4)	-0.8(-0.7)
NGC4697-49	12:48:31.0	-05:48:28	11.8	3.1	7.0	2.5	2.3	1.0	-0.3(-0.2)	-0.7(-0.5)
NGC4697-50	12:48:40.8	-05:48:22	13.1	3.3	2.8	1.2	1.4	0.6	-0.7(-0.6)	-0.8(-0.6)
NGC4697-59	12:48:32.9	-05:46:14	11.4	3.3	7.9	2.7	1.8	0.8	-0.2(-0.2)	-0.7(-0.6)
NGC4697-66	12:48:41.4	-05:46:02	16.4	3.9	12.1	3.4	2.3	1.0	-0.2(-0.1)	-0.8(-0.6)
NGC4697-74	12:48:28.7	-05:50:25	23.4	4.4	9.1	2.9	9.1	0.9	-0.4(-0.4)	-0.8(-0.7)
QSS-FNOH										
NGC4697-68	12:48:25.5	-05:48:08	7.6	2.5	6.7	2.4	0.5	0.2	0.0(0.0)	-0.9(-0.6)
QSS-σ										
NGC4697-64	12:48:34.4	-05:50:14	51.2	6.9	23.6	4.8	3.2	1.2	-0.4(-0.4)	-0.9(-0.8)

^a(M-S)/(M+S); value in parentheses is the maximum of HR1.

^b(H-S)/(H+S); value in parentheses is the maximum of HR2.

TABLE 6
SPECTRAL FITS TO THE BRIGHTEST SSSS AND QSSS

ID	N_H (10^{21} cm^{-2})	kT ^a (eV)	kT _{RS} ^b (keV)	α ^c	χ^2_{ν}/dof	Flux ^d	L_X ^e
SSS-HR							
M101-104	$1.16^{+1.08}_{-0.44}$	67^{+8}_{-14}			1.39/9	2.11	0.74, 1.13
M101-51	$2.14^{+0.83}_{-0.19}$	50^{+3}_{-12}			0.57/7	6.19	2.16, 3.32
M101-18	1 (fixed)	71^{+8}_{-19}			0.96/13	1.02	0.35, 0.55
M101-102	$1.54^{+0.19}_{-0.31}$	91^{+7}_{-4}	$0.74^{+0.04}_{-0.05}$		1.18/75	82.67	28.8, 44.4
M83-50	$0.24^{+0.74}_{-0.74}$	66^{+10}_{-13}			1.24/5	1.14	0.28, 0.30
M83-54	$0.95^{+0.38}_{-0.69}$	71^{+10}_{-16}			0.66/7	2	0.50, 0.53
M83-79	$2.1^{+3.74}_{-1.53}$	86^{+27}_{-30}			0.33/5	4	1, 1.1
M51-12	$0.5^{+0.93}_{-0.46}$	102^{+12}_{-16}			1.12/15	6.17	4.38, 5.20
NGC4697 (3 sources)	$0.50^{+1.31}_{-0.37}$	81^{+11}_{-7}			0.66/6	1.89	3.10, 12.28
SSS-3σ							
M83 (18 sources)	$1.83^{+1.66}_{-0.88}$	124^{+21}_{-24}			1.05/17	9.01	2.25, 2.38
QSS-MNOH							
M101-114	$4.4^{+2.33}_{-1.52}$	124^{+27}_{-25}			0.91/16	9.0	3.14, 4.83
M101-116	1 (fixed)	158^{+27}_{-27}			1.34/10	0.45	0.05, 0.08
M83-35	$2.59^{+7.6}_{-1.52}$	138^{+37}_{-76}			1.03/11	9.47	2.37, 2.50
QSS-FNOH							
M51 (3 sources)	$4.46^{+5.39}_{-4.55}$	110^{+60}_{-110}			0.97/4	35.4	25.1, 29.9
QSS-SNOH							
M101 (3 sources)	$1.20^{+1.09}_{-0.48}$			$3.20^{+1.32}_{-0.40}$	1.06/10	1.15	0.40, 0.62
QSS-σ							
M101-53	$6.72^{+1.13}_{-2.45}$		$0.64^{+0.10}_{-0.07}$		1.18/7	2.01	0.7, 10.8
M51-10	0.2 (fixed)	222^{+26}_{-23}			1.16/13	4.69	3.33, 3.96
M83-105	$2.76^{+3.42}_{-1.93}$	165^{+45}_{-35}			1.13/5	1.36	0.34, 0.36
M83-116	$2.14^{+1.63}_{-1.63}$	146^{+45}_{-35}			1.55/25	6.17	1.54, 1.63
M83-117 ^f	$4.82^{+0.81}_{-1.31}$	54^{+18}_{-15}	0.51 ± 0.05 ^g		1.31/19	75.6	18.9, 20
M83-119	$2.77^{+3.26}_{-1.43}$	132^{+27}_{-37}			1.24/20	6.5	1.62, 1.72
QSS-NOH							
M83 (6 sources)	$0.74^{+3.66}_{-0.74}$	172^{+74}_{-74}			0.57/5	0.95	0.24, 0.25
QSS-HR₁							
M83-120 ^f	1 (fixed)	56^{+3}_{-4}	$0.68^{+0.06}$ ^g		0.62/14	4.74	1.18, 1.25

Note. — All quoted uncertainties are 90% confidence. The ACISABS model was applied to correct for the degradation of ACIS (see text).

^aBlackbody temperature.

^bRaymond-Smith temperature.

^cPower-law photon index.

^dUnabsorbed flux ($\times 10^{-14} \text{ erg cm}^{-2} \text{ s}^{-1}$) in 0.3–7 keV.

^eLuminosity ($\times 10^{38} \text{ erg s}^{-1}$) in 0.3–7 keV. The upper and lower limits quoted here are based on the farthest and nearest distances, respectively, shown in Table 2.

^fBackground (diffuse emission) not subtracted.

^gMEKAL plasma temperature.

TABLE 7
CENTRAL CONCENTRATION OF VSSS

Galaxy	f_{VSS}	f_{all}	f_{area}	$\mathcal{F}_{VSS} = f_{VSS}/f_{area}$	$\mathcal{F}_{all} = f_{all}/f_{area}$
M101	0.09	0.08	0.006	15	13
M83	0.20	0.18	0.004	50	45
M51	0.05	0.04	0.001	50	40
NGC4697	0.36	0.14	0.001	360	140

Note. — f_{VSS} : Fraction of VSSs in the central 1 kpc; f_{all} Fraction of all X-ray sources in the central 1 kpc; f_{area} : fraction of the galaxy's total surface area comprised by a 1 kpc radius disk.

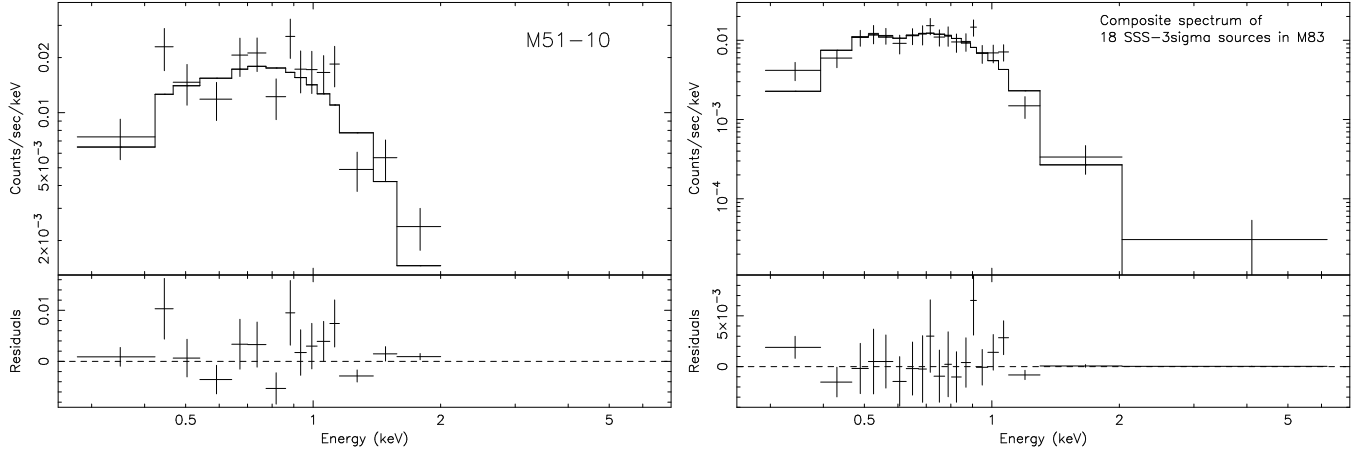


FIG. 1.— Left: Blackbody spectral fit to QSS- σ M51-10 ($N_H = 2 \times 10^{20} \text{ cm}^{-2}$, $kT = 222 \text{ eV}$). Right: Composite spectrum ($N_H = 1.8 \times 10^{21} \text{ cm}^{-2}$, $kT = 124 \text{ eV}$) of 18 SSS- 3σ sources in M83. Fits to other SSSs are shown in Di Stefano and Kong (2003b).

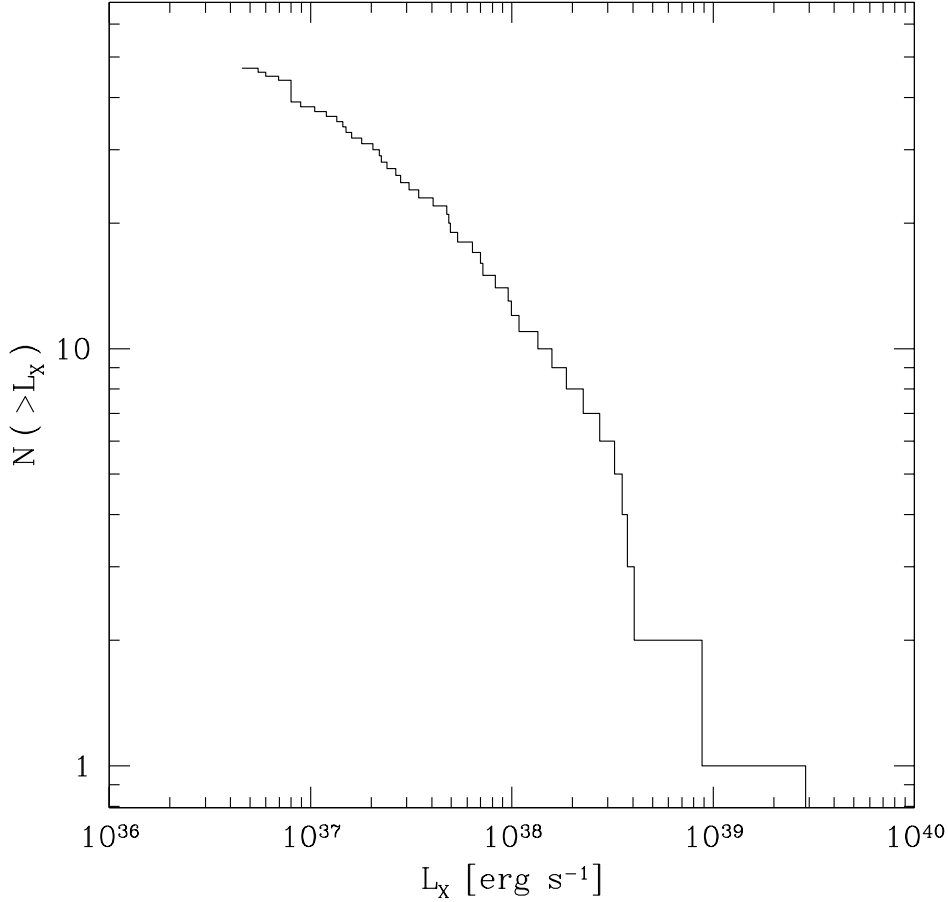


FIG. 2.— Cumulative luminosity function of all VSSs for which we have spectral fits. (See Table 6 and §2.2.1.) The luminosities are based on the lower limit of the distance estimation for the galaxy listed in Table 1. The brightest source is M101-102, with a high (low) luminosity of $4.4 \times 10^{39} \text{ ergs s}^{-1}$ ($2.9 \times 10^{39} \text{ ergs s}^{-1}$).

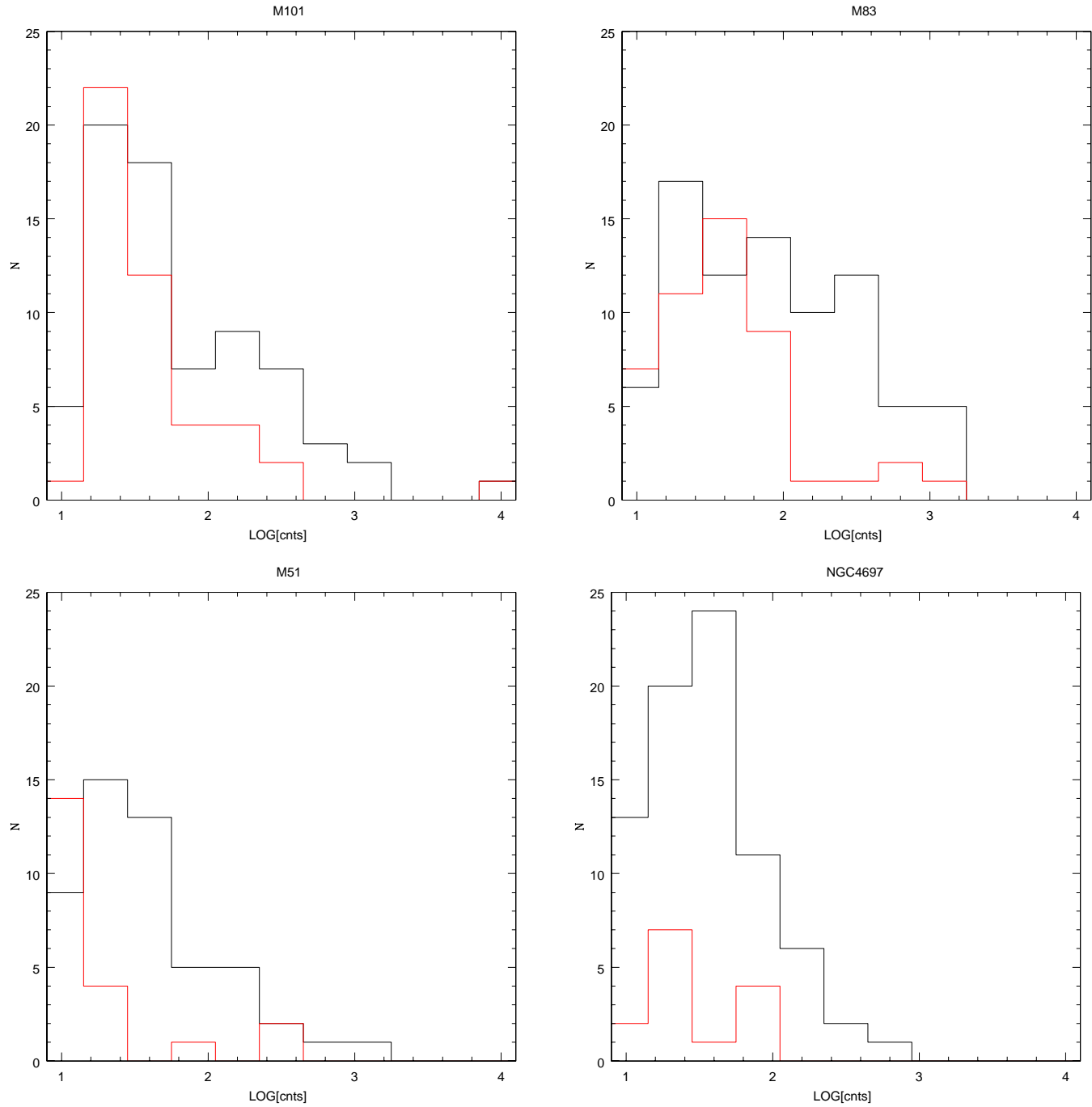


FIG. 3.— Histograms of total counts for each galaxy. Red: VSSs; black: non-VSSs. See §5.3.2.

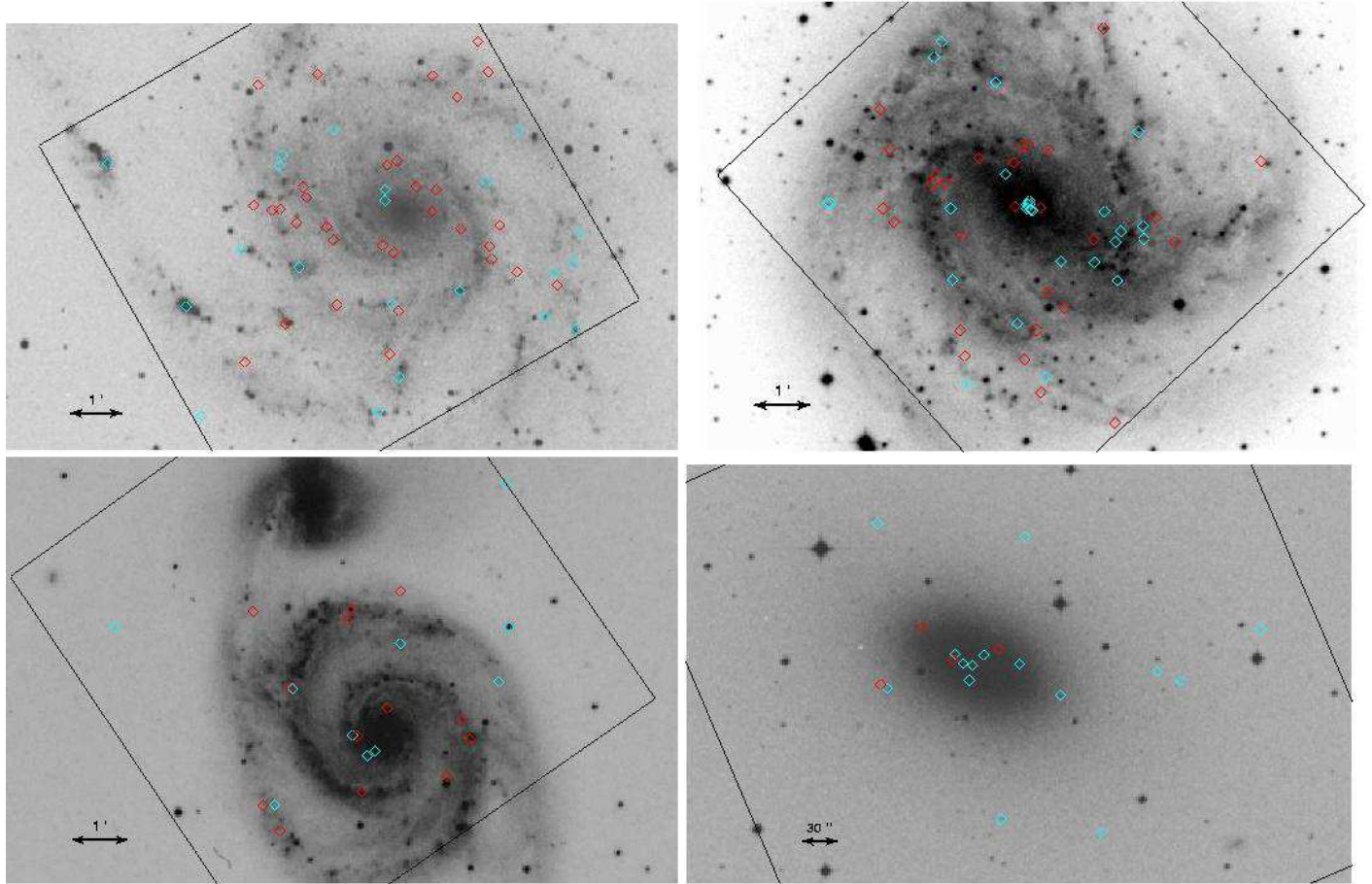


FIG. 4.—*Chandra* field-of-view (ACIS-S3; black line) overlaid on the Digital Sky Survey images of M101 (upper left), M83 (upper right), M51 (lower left) and NGC4697 (lower right). Also shown in the figures are the positions of all very soft X-ray sources (SSSs: red; QSSs: cyan).

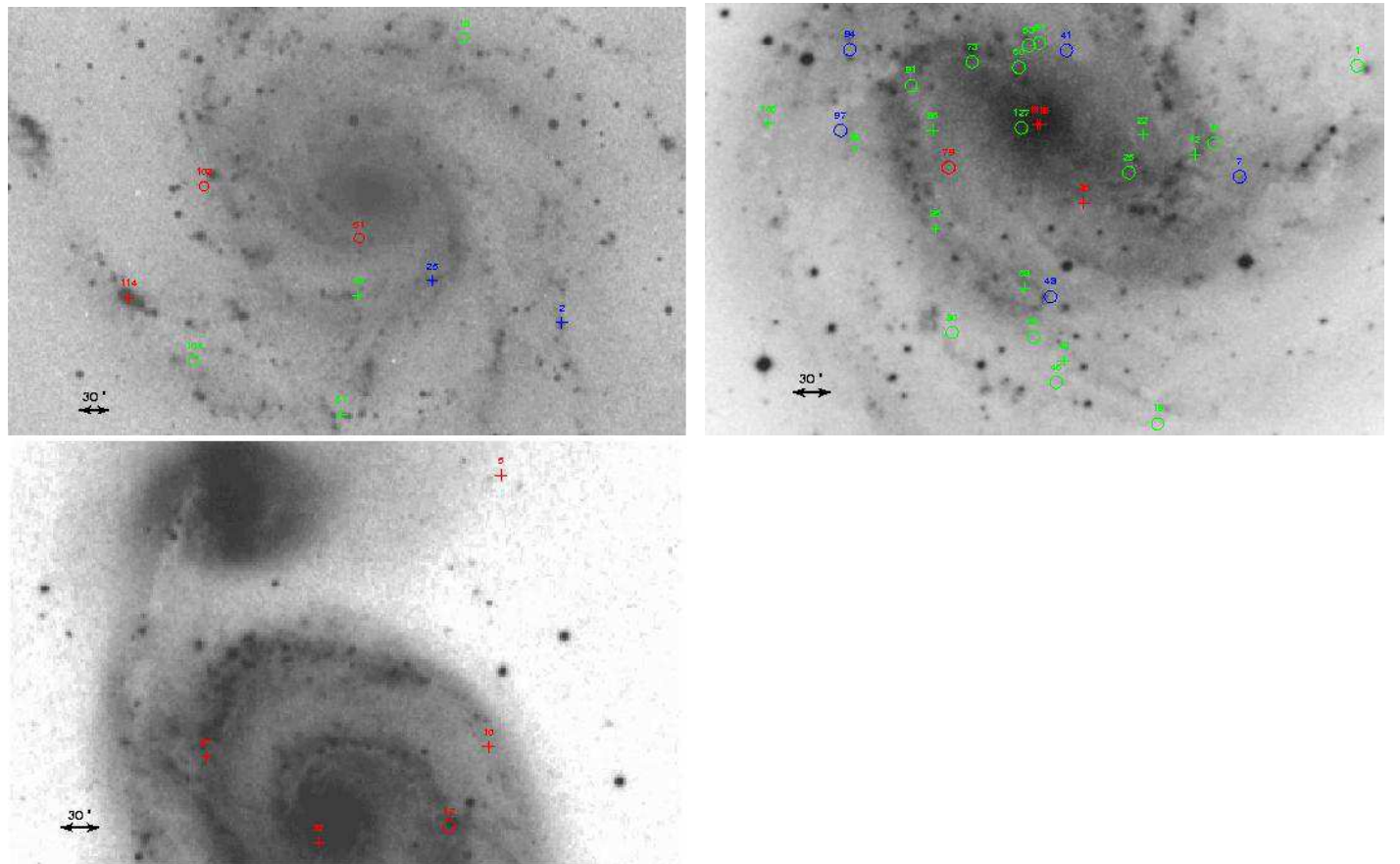


FIG. 5.— Very soft sources which provided enough photons to allow spectral fits. The galaxies are arranged as in Figure 10. Red: luminosity above 10^{38} erg s $^{-1}$; green: luminosity between 10^{37} erg s $^{-1}$ and 10^{38} erg s $^{-1}$; blue: luminosity between 10^{36} erg s $^{-1}$ and 10^{37} erg s $^{-1}$) in M101, M83 and M51. Circles represent SSSs while crosses are QSSs. The number is the source number listed in Table 2, 3, and 4.

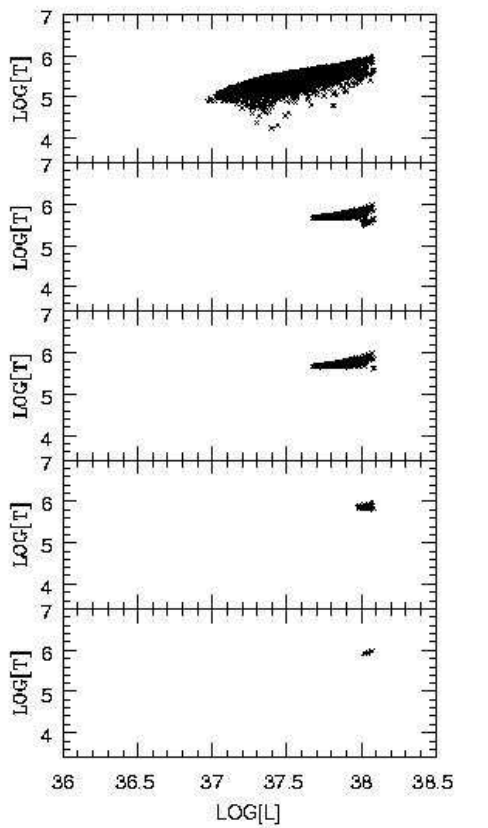


FIG. 6.— $\text{Log}[T]$ vs $\text{Log}[L]$ for (top panel) all “classical” SSSs from an RDS distribution (see §6); those members of the distribution detected and selected as SSSs in M101, M83, M51, and NGC 4697 (successive lower panels).